

Technische Universität Berlin
Institut für Strömungsmechanik und Technische Akustik
Fachgebiet Numerische Fluidodynamik

Exponentially-Fitted Finite Volume Methods for Population Balance Systems

Viktor Brilz
25. April 2016

Masterarbeit
Physikalische Ingenieurwissenschaft

Betreuer: Prof. Dr. Volker John
Erstgutachter: Prof. Dr. Jörn Sesterhenn

Eidesstattliche Versicherung

Hiermit erkläre ich, dass ich die vorliegende Arbeit selbstständig und eigenhändig sowie ohne unerlaubte fremde Hilfe und ausschließlich unter Verwendung der aufgeführten Quellen und Hilfsmittel angefertigt habe.

Berlin, den 25. April 2016

.....
Viktor Brilz

Contents

1	Introduction	6
2	Mathematical Modeling	8
2.1	Navier-Stokes Equations	9
2.2	The Population Balance Equation	13
2.3	Phase Variables	17
2.4	Population Balance System	20
2.5	Nondimensionalization	23
2.6	Cylindrical coordinates	25
3	The Finite Volume Method	32
3.1	Preliminaries	32
3.2	An introductory example: The Heat Equation	33
3.3	The convection-diffusion-reaction equation	34
3.4	The exponentially fitted upwind scheme	38
3.5	The population balance equation	39
3.6	Evaluation of the Aggregation Functional	42
4	Numerical Experiments	45
4.1	Linear Solution	46
4.2	Quadratic Solution	47
4.3	Heat equation with multiple Fourier series	49
4.4	Sharp layers	51
4.5	Numerical Solution of the Population Balance System	54
5	Conclusions and Outlook	57
	Zusammenfassung	60

1 Introduction

Population balances are widely used in different fields of science and engineering, such as chemical engineering, geophysics, biophysics and the pharmaceutical industry. Their applications range from crystallization processes to cell growth of biological cultures to the prediction of smoke particles after a volcanic eruption. All these fields have in common that particles are dispersed in another phase. But, compared to fluids in continuum mechanics, particles may undergo new phenomena: they may grow or shrink; they can be destroyed or created; a collection of particles may be bound together by interparticle forces and behave like an individual one, referred to as an *aggregate* or *agglomerate*. These phenomena usually depend on other variables in addition to location and time, such as the particle diameter in crystallization processes or the age of biological cells. One refers to them as *internal coordinates* as apposed to external (space) coordinates. The function sought here is the so-called *particle size distribution* or number density. Integrating this number density over some volume gives the number of particles contained in that volume in dependence of the internal coordinates. Taking all these effects into account one gets a *population balance equation*. Consequently, population balances play the same role that conservation laws play in continuum mechanics and thus are fundamental for the theoretical understanding of the underlying processes.

The dependence on internal coordinates as well as the new phenomena pose a great challenge in several ways. First, the internal variables add more dimensions and therefore increase the complexity; second, appropriate models describing the additional phenomena have to be found, which can be a very demanding task. Third, many of these models involve the integration of the particle size distribution such that the type of the equation is changed to a partial integro-differential equation. This makes the mathematical analysis in a lot of cases unfeasible. From a numerics point of view, both the extra dimensions and the integral terms require specialized methods: On one hand the computational costs scale exponentially with the dimension, on the other hand the integral has to be evaluated in every point in space and time. Furthermore, influences from the fluid have to be taken into account, so additional equations and constraints regarding the choice of numerical methods appear. This leads to a *population balance system*.

So far rather statistical methods have been used for the numerical simulation of population balance systems, by which the model is simplified, and, instead of solving the higher dimensional equation, a system of equations defined only in space and time is solved. The most widely spread are the quadrature method of moments (see McGraw [22]) and the direct quadrature method of moments (see Marchisio and Fox [21]), approximating the first moments of the function sought. Unfortunately, this is an ill-posed problem, see John et al. [14] and Souza et al. [31]. Following the approach of Hackbusch et al. [10] and Anker et al. [1], in this work the population balance system is solved directly without further simplifications. Since there is no analytical solution available, an experiment is used to validate the numerically obtained solution. In this experiment there are urea particles dispersed in ethanol, flowing through a tube.

The objective of this thesis is the implementation of a finite volume method solving the population balance equation for the particle size distribution in the software system MooNMD at the Weierstrass Institute for Applied Analysis and Stochastics. Finite difference methods for solving population balance equations are already available. Finite

volume methods are attractive as they can be extended to be suitable for complex geometries and have certain desirable properties like mass conservation.

The thesis is organized as follows: **Chapter 2** is concerned with the mathematical modeling of the population balance system and a derivation of the equations is provided. Subsequently, the equations are nondimensionalized, transformed into an appropriate coordinate system and summarized for future reference. **Chapter 3** presents the finite volume method applied to different types of equations. As no results concerning analytical solutions of the resulting population balance system could be found, the numerical analysis is omitted here. **Chapter 4** contains several numerical experiments as well as the discussion of properties of interest of the obtained solutions. Furthermore the result of this thesis is presented: The numerical solution of the population balance system. A brief description of the experiment together with the measured quantity is given as well as an overview of the numerical methods used to solve the other equations. **Chapter 5** summarizes the conclusion and gives a brief outlook.

2 Mathematical Modeling

This chapter is devoted to the mathematical modeling of natural processes that appear in this work. First, we start with the hypothesis of the continuum theory since this is fundamental to the whole thesis and derive a generic conservation equation. Next, we use that conservation equation to derive all equations concerning the continuous phase such as the Navier-Stokes equations that govern fluid flow. Lastly, and most importantly, we will focus on population balances where an introduction will be given because it is usually not covered in lectures and, therefore, not widely known. At the end of this chapter we will state the full problem which will be solved numerically and discuss physical and chemical quantities together with their influence on the system.

Continuum theory as used in continuum mechanics is a physical model where the structure and spatial distribution of atoms and molecules of media is not taken into account. Instead, it is assumed that the media exists continuously and is defined for any point within the space under consideration. This assumption is justified because not the individual behavior of each molecule, but rather of the whole system is of interest. Moreover, measuring instruments respond to properties of the fluid within a small neighboring volume; this volume is small enough to be ‘local’ compared to macroscopic forces like gravity, but still very large compared to microscopic length scales of molecules. Figure 2.1 illustrates the density an instrument would measure depending on the size of the neighboring volume. One can see that the measured density depends neither on the microscopic differences nor on the spatial distribution of density in a certain range of length (between 10^{-7} m and 10^{-3} m, see Schade et al. [28, chapter 1.6]).

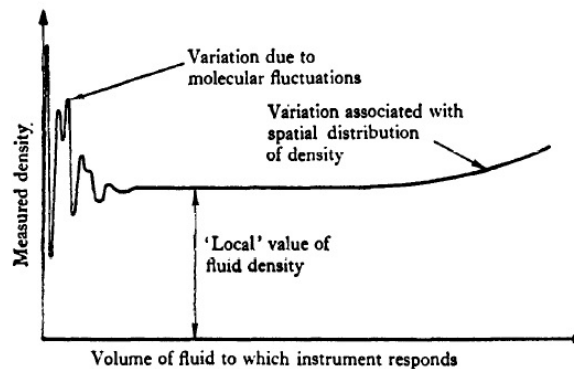


Figure 2.1: Effect of size of volume on the density measured by an instrument (Batchelor [2, chapter 1.2]).

The *fluid* is a physical model widely used to describe liquids and gases theoretically. Every fluid is defined as being a continuum upon which, when at rest, only pressure can be applied, but neither shear stresses nor tensile forces. Due to its continuous nature, calculus may be applied, leading to partial differential equations governing its behavior. Most of the identities of this chapter are based on a book written by Gurtin et al. [7], which forms a resource for extensive and thorough derivations of equations in continuum mechanics. Note that in general we will make no smoothness hypotheses as the focus in this chapter lies on the modeling and derivation of equations governing natural processes. Thus, all appearing functions are assumed to be as often differentiable as necessary.

Let ψ be a function. Usually it will be some sort of density, for instance, the mass density ρ . Then, integrated over some volume $\Omega \subset \mathbb{R}^3$, it contains the amount of the physical entity within that volume, i.e.,

$$\int_{\Omega} \psi \, dx.$$

Consider also the set to be time-dependent: $\Omega(t)$. In the literature it is referred to as *material volume* because the region moves with the portions it is made of. The fundamental concept of conservation laws is based on *Reynolds transport theorem*, which describes the rate of change of an entity in the case that both the volume and the function are time-dependent. Normally it is stated in three dimensions since continuum mechanics typically deals with bodies that are independent of other variables but the location (and time) or where such dependencies are neglected. As we will see, population balances require a generalization to higher dimensions. Therefore, we formulate the theorem accordingly.

Reynolds Transport Theorem

Let $\psi(\mathbf{x}, t)$ be a differentiable function over $\Omega(t) \times [0, \infty)$ where it may be scalar, vector, or tensor valued and $\Omega(t) \subset \mathbb{R}^d, d \geq 2$. Furthermore, consider the velocity $\mathbf{u} = (dx/dt, dy/dt, dz/dt)^T$ as a differentiable function over the same domain. Then there holds:

$$\frac{d}{dt} \int_{\Omega(t)} \psi(\mathbf{x}, t) \, d\mathbf{x} = \int_{\Omega(t)} (\partial_t \psi(\mathbf{x}, t) + \operatorname{div}(\psi(\mathbf{x}, t)\mathbf{u}(\mathbf{x}, t))) \, d\mathbf{x}. \quad (2.1)$$

Note that the classic formulation of the theorem

$$\frac{d}{dt} \int_{\Omega(t)} \psi(\mathbf{x}, t) \, d\mathbf{x} = \int_{\Omega(t)} \partial_t \psi(\mathbf{x}, t) \, d\mathbf{x} + \int_{\partial\Omega(t)} \psi(\mathbf{x}, t)\mathbf{u}(\mathbf{x}, t) \cdot \mathbf{n}(\mathbf{x}, t) \, dS(\mathbf{x})$$

may be recovered if one splits the right-hand side into two integrals and applies Gaussian's divergence theorem to the second integral.

Central in the proof of this theorem is the substitution rule and Jacobi's formula which gives an equation for the derivative of the determinant of a matrix, see also the book of Gurtin et al. [7]. In subsequent sections we will make extensive use of this theorem to derive various conservation and balance laws.

2.1 Navier-Stokes Equations

The Navier-Stokes equations consist of a scalar equation for the conservation of mass and a vector equation for the momentum balance.

Conservation of mass

In order to obtain the equation for the conservation of mass we choose $\psi = \rho$, ρ [kg/m³] being the density of the fluid, and consider an arbitrary subset $\omega(t) \subset \Omega(t)$. Since mass can neither be destroyed nor created, the mass inside a material volume does not change with respect to time:

$$\frac{d}{dt} \int_{\omega(t)} \rho(\mathbf{x}, t) \, d\mathbf{x} = 0.$$

Using Reynolds transport theorem (2.1) yields

$$\frac{d}{dt} \int_{\omega(t)} \rho(\mathbf{x}, t) d\mathbf{x} = \int_{\omega(t)} (\partial_t \rho(\mathbf{x}, t) + \operatorname{div}(\rho(\mathbf{x}, t)\mathbf{u}(\mathbf{x}, t))) d\mathbf{x}.$$

Since the volume is arbitrary and the integrand continuous, the integral vanishes if and only if the integrand is zero which leads to the so-called **continuity equation**:

$$\partial_t \rho(\mathbf{x}, t) + \operatorname{div}(\rho(\mathbf{x}, t)\mathbf{u}(\mathbf{x}, t)) = 0.$$

Rewritten in a more compact manner and omitting the dependencies on location and time:

$$\partial_t \rho + \operatorname{div}(\rho\mathbf{u}) = 0. \quad (2.2)$$

Thus far we have used kinematic arguments only without any restraints on the material under consideration. Now we employ the model of an *incompressible fluid* in which the density is constant with respect to time and location. Note that this does not exclude the case where it depends on the temperature (which would be quite realistic). But in fluid dynamics it is common to neglect this case and assume an *isothermal* flow as it is either not significant or it would result in a extremely complicated model which is nearly unfeasible to solve. This leads to

$$\begin{aligned} \partial_t \rho + \operatorname{div}(\rho\mathbf{u}) &= \underbrace{\partial_t \rho}_{=0} + \underbrace{\nabla \rho \cdot \mathbf{u}}_{=0} + \rho \operatorname{div} \mathbf{u} = 0 \\ &\Leftrightarrow \operatorname{div} \mathbf{u} = 0. \end{aligned} \quad (2.3)$$

Therefore, in the case of an incompressible fluid, the continuity equation degenerates to a constraint on the velocity.

Balance of linear momentum

The derivation in the case of linear momentum proceeds in the same fashion but is somewhat more complicated and is no conservation because the momentum of a material volume may change with time since it is based on *Newton's second law*: the rate of change of momentum of a material volume equals the sum of the forces acting upon it. In continuum mechanics there are two different types of forces acting on a material volume: long range or body forces, which act on the whole volume, and short range or surface forces, which act only on the surface, such that Newton's second law reads for an incompressible fluid as follows:

$$\frac{d}{dt} \int_{\omega(t)} \rho\mathbf{u} d\mathbf{x} = \int_{\omega(t)} \rho\mathbf{f} d\mathbf{x} + \int_{\partial\omega(t)} \mathbf{t} dS(\mathbf{x}). \quad (2.4)$$

The body forces are represented by \mathbf{f} and the surface forces by \mathbf{t} . First we consider the momentum only and deal with the forces afterwards. We choose $\psi = \rho\mathbf{u}$ since it represents a 'momentum density', i.e., momentum per volume and again we use Reynolds transport theorem:

$$\frac{d}{dt} \int_{\omega(t)} \rho\mathbf{u} d\mathbf{x} = \int_{\omega(t)} (\partial_t(\rho\mathbf{u}) + \operatorname{div}(\rho\mathbf{u} \otimes \mathbf{u})) d\mathbf{x},$$

where $\mathbf{u} \otimes \mathbf{u}$ denotes the dyad product resulting in a second order tensor. The divergence of a second order tensor results in a vector. Stating the tensor in coordinates, computing the derivatives, and restating it in direct notation one obtains:

$$\operatorname{div}(\mathbf{u} \otimes \mathbf{u}) = \mathbf{u} \operatorname{div} \mathbf{u} + \mathbf{u} \cdot \nabla \mathbf{u}.$$

Making use of the incompressibility of the fluid, namely that ρ is independent of location and time and $\operatorname{div} \mathbf{u} = 0$, one gets

$$\frac{d}{dt} \int_{\omega(t)} \rho \mathbf{u} \, d\mathbf{x} = \int_{\omega(t)} (\rho \partial_t \mathbf{u} + \rho \mathbf{u} \cdot \nabla \mathbf{u}) \, d\mathbf{x}. \quad (2.5)$$

Now we turn to the forces: \mathbf{f} has the dimension of an acceleration [m/s²] and can be considered as a ‘force density’. For our considerations it will only represent the gravitational force, i.e., $\mathbf{f} = \mathbf{g}$ with $\mathbf{g} = (0, 0, -9.81)^T$ being the gravitational acceleration. \mathbf{t} on the other side has the dimension of pressure or, more general, mechanical stress [N/m²]. We make use of *Cauchy’s fundamental postulate* (see Itskov [13], section 1.6) which states that \mathbf{t} is a function of location \mathbf{x} , time t , and the outward unit normal vector of the surface \mathbf{n} only where the dependency with respect to \mathbf{n} is linear:

$$\mathbf{t}(\mathbf{x}, t, \mathbf{n}) = \boldsymbol{\sigma}(\mathbf{x}, t) \mathbf{n}. \quad (2.6)$$

The second order tensor $\boldsymbol{\sigma}$ [N/m²] is called **stress tensor**. One can show (via an angular momentum balance) that the stress tensor is symmetrical, i.e., $\sigma_{ij} = \sigma_{ji}$, $1 \leq i, j \leq 3$. As mentioned above, a fluid does not experience any shear stresses at rest, therefore we model the stress tensor accordingly:

$$\boldsymbol{\sigma} = -p \boldsymbol{\delta} + \boldsymbol{\tau}, \quad \sigma_{ij} = p \delta_{ij} + \tau_{ij},$$

where p [N/m²] is the **pressure**, $\boldsymbol{\tau}$ [N/m²] is the so-called **viscous stress tensor** and is equal to zero if the fluid is at rest. Note that $\boldsymbol{\tau}$ is symmetrical which is inherited from $\boldsymbol{\sigma}$ and has zero trace. It is not possible to state a general term for it holding true for all materials but quite the contrary, as one has to adapt it to every single model. Therefore, we define our model further and consider from now on a **Newtonian fluid**: We say that the viscous stress tensor $\boldsymbol{\tau}$ is approximately a linear function of the velocity gradient $\nabla \mathbf{u}$. Since $\boldsymbol{\tau}$ as well as $\nabla \mathbf{u}$ are second order tensors they are linked by a fourth order tensor:

$$\boldsymbol{\tau} = \boldsymbol{\eta} : \nabla \mathbf{u}, \quad \tau_{ij} = \sum_{k,l=1}^3 \eta_{ijkl} \partial_{x_k} u_l, \quad (2.7)$$

where “:” represents the double scalar product and $\boldsymbol{\eta}$ [N s/m²] is called **viscous tensor**. This tensor has to be symmetrical in i and j because $\boldsymbol{\tau}$ is symmetrical. Moreover, we assume the medium to be **isotropic**, that is, when the viscous stress generated in an element of the fluid by a given velocity gradient is independent of the orientation of the element. This results in $\boldsymbol{\eta}$ being isotropic as well. One can show that a general isotropic fourth order tensor can be represented in the following way:

$$\eta_{ijkl} = a \delta_{ij} \delta_{kl} + b \delta_{ik} \delta_{jl} + c \delta_{il} \delta_{jk},$$

with $a, b, c \in \mathbb{R}$. (Note that in case the viscosity depends on location or time, the coefficients would be functions.) Since $\boldsymbol{\eta}$ is symmetrical in i and j , we require $b = c$. Renaming

b and a by μ and μ' , respectively, inserting the relation above into Equation (2.7), and exploiting the properties of Kronecker delta tensors, we obtain

$$\tau_{ij} = \sum_{k,l=1}^3 (\mu' \delta_{ij} \partial_{x_k} u_k + \mu (\partial_{x_i} u_j + \partial_{x_j} u_i))$$

or in symbolic notation

$$\boldsymbol{\tau} = \mu' (\operatorname{div} \mathbf{u}) \boldsymbol{\delta} + \mu (\nabla \mathbf{u} + (\nabla \mathbf{u})^T).$$

From the mass conservation for an incompressible fluid we know that the velocity is divergence-free, yielding:

$$\boldsymbol{\tau} = \mu (\nabla \mathbf{u} + (\nabla \mathbf{u})^T).$$

With that we arrive at the final model for the stress tensor of a Newtonian fluid:

$$\boldsymbol{\sigma} = -p \boldsymbol{\delta} + \mu (\nabla \mathbf{u} + (\nabla \mathbf{u})^T), \quad (2.8)$$

where μ is the **dynamic viscosity**. Inserting this and Equations (2.5) and (2.6) into Equation (2.4) leads to

$$\int_{\omega(t)} (\rho \partial_t \mathbf{u} + \rho \mathbf{u} \cdot \nabla \mathbf{u}) \, d\mathbf{x} = \int_{\omega(t)} \rho \mathbf{g} \, d\mathbf{x} + \int_{\partial\omega(t)} (-p \boldsymbol{\delta} + \mu (\nabla \mathbf{u} + (\nabla \mathbf{u})^T)) \cdot \mathbf{n} \, dS(\mathbf{x}).$$

Applying Gaussian's divergence theorem once more and putting all terms on one side we obtain

$$\begin{aligned} 0 &= \int_{\omega(t)} (\rho \partial_t \mathbf{u} + \rho \mathbf{u} \cdot \nabla \mathbf{u} - \rho \mathbf{g} - \operatorname{div} (-p \boldsymbol{\delta} + \mu (\nabla \mathbf{u} + (\nabla \mathbf{u})^T))) \, d\mathbf{x} \\ &= \int_{\omega(t)} \left(\rho \partial_t \mathbf{u} + \rho \mathbf{u} \cdot \nabla \mathbf{u} - \rho \mathbf{g} + \nabla p - \mu \left(\Delta \mathbf{u} + \nabla \underbrace{\operatorname{div} \mathbf{u}}_{=0} \right) \right) \, d\mathbf{x} \\ &= \int_{\omega(t)} (\rho \partial_t \mathbf{u} + \rho \mathbf{u} \cdot \nabla \mathbf{u} - \rho \mathbf{g} + \nabla p - \mu \Delta \mathbf{u}) \, d\mathbf{x}. \end{aligned}$$

Because of the continuity of the integrand we conclude that the integrand has to vanish equally, yielding:

$$\rho \partial_t \mathbf{u} - \mu \Delta \mathbf{u} + \rho \mathbf{u} \cdot \nabla \mathbf{u} + \nabla p = \rho \mathbf{g}.$$

Divided by ρ it forms together with the continuity equation the **Navier-Stokes equations** for an incompressible fluid, leading to the final equation:

$$\begin{aligned} \operatorname{div} \mathbf{u} &= 0, \\ \partial_t \mathbf{u} - \nu \Delta \mathbf{u} + \mathbf{u} \cdot \nabla \mathbf{u} + \frac{1}{\rho} \nabla p &= \mathbf{g}, \end{aligned} \quad (2.9)$$

where $\nu = \mu/\rho$ is the **kinematic viscosity**.

2.2 The Population Balance Equation

In this section we want to model the behavior of particles dispersed in a fluid. There are some major differences compared to the model given above. First, since we are dealing with particles it is not continuous media. Liquids and gases are not continuous either; we just *model* them to be continuous. The major difference is that the particles in case of liquids and gases are molecules with a diameter of about 10^{-10} to 10^{-9} m whereas the particles considered here have a diameter greater than 10^{-6} m. Moreover, the particle structure has a great impact on the behavior of the whole system. Second, the particles may experience phenomena which do not apply to fluids, for instance, growth processes. Lastly, they may depend not only on location and time, like the fluid, but also on other entities like their size or shape. We will refer to these dependencies as *internal coordinates*, collected in $\boldsymbol{\ell}$, where the spatial variables \boldsymbol{x} are called *external coordinates*. Functions, like the temperature, describing the fluid phase and depending only on the external coordinates and time are also called *phase variables*. The approach in this case is not a conservation equation but a *population balance*. The identities stated here can give little insight into the theory of population balances. It is taken from Ramkrishna [24] which contains a general introduction as well as in-depth material and forms the standard reference in the literature. For particulate processes, one should also consider Randolph and Larson [25].

In this section we will refer to the volume in (physical) space by $\Omega_x \subset \mathbb{R}^3$ and introduce a new set $\Omega_\ell \subset \mathbb{R}^r$, which represents the ‘volume’ in internal coordinates; r is a natural number representing the number of dependencies on internal coordinates. Note that we omitted in the notation the explicit dependency on time, but it should be kept in mind that all sets and subsets may still evolve with time. We will refer to the set $\Omega_x \times \Omega_\ell$ as the **particle state space** or simply state space and say that a particle is of a certain state if $(\boldsymbol{x}, \boldsymbol{\ell}) \in \Omega_x \times \Omega_\ell$. Although r will equal 1 in our final model (and ℓ the diameter of a particle), we let it be arbitrary for the derivation since it involves only already known methods from calculus but reveals some parallels.

We start with introducing the **actual number density** $n(\boldsymbol{x}, \boldsymbol{\ell}, t)$: Integrated over some subsets of Ω_x and Ω_ℓ it describes the number of particles contained in it. The term ‘actual’ comes from the fact that this density is a random variable if one considers all possible random behavior of small particles (for instance Brownian motion). We concern ourselves with a large amount of particles and, as in the case of continuum theory, we are not interested in the individual but rather the average behavior of the system. Therefore, the key function here is the expectation of the actual number density, which we will refer to as the **number density** or **particle size distribution**:

$$f : \Omega_x \times \Omega_\ell \times [0, \infty) \rightarrow \mathbb{R}, \quad f(\boldsymbol{x}, \boldsymbol{\ell}, t) := \mathbb{E}[n(\boldsymbol{x}, \boldsymbol{\ell}, t)].$$

With this definition the (average) total number of particles in the whole system is given by

$$\int_{\Omega_x} \int_{\Omega_\ell} f(\boldsymbol{x}, \boldsymbol{\ell}, t) \, d\boldsymbol{\ell} \, d\boldsymbol{x}.$$

We want to quantify the rate of change of that entity given in this system. The internal coordinates are the reason why Reynolds Transport Theorem has been stated for possibly

more than three variables. For this section we also introduce the divergence with respect to external and internal coordinates by div_x and div_ℓ , respectively. Next, influences from the fluid phase, like pressure or temperature, on the particles have to be considered. Therefore, we collect all **phase variables** in one vector function $\mathbf{Y}(\mathbf{x}, t)$; its dimension depending on how many influences will be considered in the model. Another important function is the **growth rate** $\mathbf{G}(\mathbf{x}, \ell, t, Y)$. In its general definition it may depend on external and internal coordinates as well as the time and the phase variables. Its dimension is r because it is basically the time derivative of the internal coordinates, i.e., $\mathbf{G} = d\ell/dt$. It can be interpreted as an analogue of the fluid velocity, representing an abstract velocity in the space of internal coordinates. Like the fluid velocity, it is a priori unknown and has to be either calculated or modeled.

On the left-hand side of a population balance equation one has the rate of change of the number of particles within a volume and on the right-hand side the birth and death rates of particles in that volume; more precisely, consider subsets ω_x and ω_ℓ of Ω_x and Ω_ℓ , respectively, then one has:

$$\frac{d}{dt} \int_{\omega_x} \int_{\omega_\ell} f(\mathbf{x}, \ell, t) d\mathbf{x} d\ell = \int_{\omega_x} \int_{\omega_\ell} A(\mathbf{x}, \ell, t, \mathbf{Y})[f] d\ell d\mathbf{x},$$

where $A(\mathbf{x}, \ell, t, \mathbf{Y})[f]$ accounts for birth and death rates of the population. The notation indicates that A may be a functional and also depend explicitly on the external, internal, and phase variables and time. It is highly dependent on the process under consideration and will be modeled later. Now we make use of Reynolds transport theorem (2.1) with $\psi = f$. Note that the theorem is formulated for any dimension (greater or equal to 2); so that the internal coordinates are already incorporated. Neglecting the variables for clarity leads to

$$\frac{d}{dt} \int_{\omega_x} \int_{\omega_\ell} f d\mathbf{x} d\ell = \int_{\omega_x} \int_{\omega_\ell} (\partial_t f + \text{div}_x(f\mathbf{u}) + \text{div}_\ell(f\mathbf{G})) d\mathbf{x} d\ell.$$

Subtracting the right-hand side yields

$$\int_{\omega_x} \int_{\omega_\ell} (\partial_t f + \text{div}_x(f\mathbf{u}) + \text{div}_\ell(f\mathbf{G}) - A[f]) d\mathbf{x} d\ell = 0.$$

Again, because the subsets ω_x and ω_ℓ are arbitrary, the integral can be zero only if the integrand vanishes equally. Rewriting $A[f]$ on the right-hand side results in

$$\partial_t f + \text{div}_x(f\mathbf{u}) + \text{div}_\ell(f\mathbf{G}) = A[f].$$

This is the general population balance equation for the particle size distribution and we are ready to specify our model. We assume that the particles are spherical and choose the inner variable ℓ to be the **diameter of the particles**. Hence, $\Omega_\ell = (\ell_{\min}, \ell_{\max})$ with lower and upper bounds for the smallest and largest particles, respectively. Thus the dimension of f is $[1/\text{m}^4]$ since it is the number density per (physical) volume and (internal) interval, G has the dimension of a velocity $[\text{m}/\text{s}]$, and A has the dimension $[1/(\text{m}^4 \text{s})]$. Accordingly, the population balance equation changes to

$$\partial_t f + \text{div}_x(f\mathbf{u}) + \partial_\ell(fG) = A[f]. \quad (2.10)$$

The right-hand side A is governed by *aggregation*, explained and modeled in some detail subsequently. The fluid velocity \mathbf{u} is determined by the Navier-Stokes equations (2.9) and the model for the growth rate will be given later. Note, that new particles may be formed also by *nucleation*, that is, the phenomenon when particles are created in a supersaturated solution. In an experiment they appear as the smallest particles one can resolve with a microscope. This will be also incorporated in our model, but not directly in the equation but as a boundary condition with respect to the internal coordinate.

Aggregation

In our model, the right-hand side $A[f]$ is determined by *aggregation*: It describes phenomena in which particles are attracted to each other by interparticle forces to form clusters, commonly referred to as *aggregates* or *agglomerates*, and covers the formation of rain from a cloud of very fine droplets as well as the clustering of particles in the manufacture of fine powders. One can think of two particles colliding and merging, even though there are also situations in which particles are bound together by surface forces only, without physical contact. Note that three or more particles may be involved to form an aggregate, but we restrict ourselves to sufficiently dilute systems where these cases are insignificant. First, we consider the production rate caused by aggregation; the death rate is obtained by the same approach. Hence, we split the right-hand side: $A[f] = A^+[f] + A^-[f]$.

In modeling aggregation, the so-called **aggregation frequency** plays an essential role. It represents the probability that a particle of state (\mathbf{x}, ℓ) and another particle of state (\mathbf{x}', ℓ') will aggregate at time t . In very general models it might include dependencies on physical space, time, or even phase variables. Instead, we consider a model in which it depends on the internal variable only. The population balance equation is formulated with ℓ being the diameter of a particle, but it is convenient to formulate the aggregation in terms of the volume of a particle, i.e., $\ell = V$ and $\Omega_\ell = (V_{\min}, V_{\max})$. Accordingly, we denote the aggregation frequency by $K(V, V')$. There are different models for different contributions, for instance, one for aggregation due to *Brownian motion*, which is given by

$$K_{\text{br}}(V, V') = \frac{2k_B T}{3\mu} \left(\sqrt[3]{V} + \sqrt[3]{V'} \right) \left(\frac{1}{\sqrt[3]{V}} + \frac{1}{\sqrt[3]{V'}} \right),$$

where k_B [J/K] is the Boltzmann constant and T [K] the temperature. Since we are dealing with a viscous fluid we should incorporate collisions caused by *shear stresses* as well, given by:

$$K_{\text{sh}}(V, V') = \frac{1}{k_V} \sqrt{2\nabla\mathbf{u} : \nabla\mathbf{u}} \left(\sqrt[3]{V} + \sqrt[3]{V'} \right),$$

where k_V is the volume shape factor, i.e., $k_V = \pi/6$ for spherical particles. Hence, we want to combine both models. Previous work has been done by Hackbusch et al. [10] where the following combination has been used:

$$\begin{aligned} K(V, V') &= C_{\text{br}} K_{\text{br}}(V, V') + C_{\text{sh}}(V, V') K_{\text{sh}}(V, V') \\ &= C_{\text{br}} \frac{2k_B T}{3\mu} \left(\sqrt[3]{V} + \sqrt[3]{V'} \right) \left(\frac{1}{\sqrt[3]{V}} + \frac{1}{\sqrt[3]{V'}} \right) + \frac{C_{\text{sh}}}{k_V} \sqrt{2\nabla\mathbf{u} : \nabla\mathbf{u}} \left(\sqrt[3]{V} + \sqrt[3]{V'} \right). \end{aligned} \quad (2.11)$$

In the paper the constants were calibrated for a pipe with quadratic cross-section by comparing numerical results with those gained from experiments. This was also done by

Anker et al. [1] but for a cylindrical pipe. Since the constants vary slightly, we will use the latter results as in this work also a cylindrical pipe was used:

$$C_{\text{br}} = 7 \cdot 10^3, \quad C_{\text{sh}} = 8.5 \cdot 10^{-5}.$$

These aggregation frequencies were introduced by Smoluchowski [30]. Because their derivation requires the theory of stochastic differential equations and statistical physics, which is beyond the scope of the work, we will not derive them here. An alternative derivation for the Brownian aggregation frequency is also given by Ramkrishna [24].

Next, it is necessary to define the **average number of pairs** of particles at each instance of time with specified states. Accordingly, we define the function

$$f_2(\mathbf{x}, \ell; \mathbf{x}', \ell', t) \quad \left[\frac{1}{\text{m}^8} \right]$$

to represent the average number of distinct pairs of particles at time t per unit volumes in state space located about (\mathbf{x}, ℓ) and (\mathbf{x}', ℓ') , respectively. Since the function is unknown an equation has to be formulated. That would incorporate f_3 – the average number of triples of particles – which is again, unknown. Thus, this approach would lead to an infinite hierarchy of equations – a problem known as the *closure problem*. Therefore, a closure hypothesis is needed; one is given by

$$f_2(\mathbf{x}, \ell; \mathbf{x}', \ell', t) = f(\mathbf{x}, \ell, t) f(\mathbf{x}', \ell', t). \quad (2.12)$$

This approximation is rather coarse because it implies that the particles under consideration are statistically uncorrelated. More complex models are stated by Ramkrishna [24] and analyzed in detail by Sampson and Ramkrishna [27]. Since we chose the volume of a particle to be the inner variable for the aggregation frequency, but formulated the population balance equation with ℓ being the diameter of a particle, we need a transformation, given by

$$f_V(\mathbf{x}, V, t) = f_V(\mathbf{x}, k_V \ell^3, t) = \frac{f(\mathbf{x}, \ell, t)}{3k_V \ell^2} \quad \left[\frac{1}{\text{m}^6} \right]. \quad (2.13)$$

Combining Equations (2.11), (2.12), and (2.13) yields the production rate caused by aggregation

$$A^+(V)[f_V] = \frac{1}{2} \int_0^V K(V - V', V') f_V(\mathbf{x}, V - V', t) f_V(\mathbf{x}, V', t) dV'. \quad (2.14)$$

The factor $1/2$ accounts for redundancies since there are two realizations of the event: One particle has volume V' and the other $V - V'$ and vice versa.

Similar considerations lead to the death term caused by aggregation since aggregating particles vanish to create a new particle; given by:

$$A^-(V)[f_V] = -f_V(V) \int_0^{V_{\text{max}}} K(V, V') f_V(V') dV'. \quad (2.15)$$

For the formulation of the population balance equation we need to express the birth and death rate with respect to the particle diameter:

$$A^+(\ell)[f] + A^-(\ell)[f] = 3k_V\ell^2 (A^+(V)[f_V] + A^-(V)[f_V]). \quad (2.16)$$

Since the right-hand side is determined, the only missing part of the equation is the growth rate G . It is given by (see Hackbusch et al. [10])

$$G(c, T) = \begin{cases} k_g \left(\frac{c - c_{\text{sat}}(T)}{c_{\text{sat}}(T)} \right)^g & \text{if } c > c_{\text{sat}}(T), \\ 0 & \text{else,} \end{cases} \quad (2.17)$$

where $k_g = 10^{-7}$ [m/s] is the growth rate constant and $g = 0.5$ [·] the growth rate power. The concentration distribution of the urea particles in ethanol is described by $c = c(\mathbf{x}, t)$ and the *saturation concentration* by $c_{\text{sat}}(T)$. The latter is given by (see Hackbusch et al. [10])

$$c_{\text{sat}}(T) = \frac{35.364 + 1.305(T - 273.15)}{m_{\text{mol}}} \left[\frac{\text{mol}}{\text{m}^3} \right] \quad (2.18)$$

and represents the condition when no more urea can be solved in ethanol. That means particles may only grow if the concentration of particles is sufficiently high. Here, $T = T(\mathbf{x}, t)$ [K] represents the temperature distribution of ethanol. Since the temperature as well as the concentration distribution are not given, they have to be determined. Depending on the model, it is quite common that additional equations for phase variables with a population balance have to be formulated and solved in order to predict the behavior of the overall system. In fact, we already encountered phase variables in the previous section: the velocity \mathbf{u} and the pressure p . The missing equations will be derived in the next section, but now we are able to state the final population balance equation for the particle size distribution of urea particles:

$$\partial_t f + \mathbf{u} \cdot \nabla f + G(c, T)\partial_\ell f = A^+[f] + A^-[f], \quad (2.19)$$

where the birth and death rate as well as the growth rate are given by Equations (2.14) to (2.17).

2.3 Phase Variables

Since the growth rate of urea particles depends on the temperature of the surrounding fluid and the concentration of particles, corresponding equations are necessary and are the object of this section. The basic concepts of this section can be found in the extensive resource for transport phenomena written by Bird et al. [3].

Temperature

For the temperature a balance of thermal energy is suitable. First we need the *thermal energy* contained in a volume:

$$\int_{\Omega(t)} \rho c_p T(\mathbf{x}, t) d\mathbf{x},$$

where ρ is the (constant) density of the fluid (which we already encountered when the Navier-Stokes equations were derived), c_p [J/(kg K)] the (constant) **heat capacity**, and

T the temperature. The rate of change of thermal energy is equal to the heat flux across the boundary:

$$\frac{d}{dt} \int_{\Omega(t)} \rho c_p T \, d\mathbf{x} = - \int_{\partial\Omega(t)} \mathbf{q} \cdot \mathbf{n} \, dS(\mathbf{x})$$

with the **heat flux vector** \mathbf{q} [J/(m² s)], representing the local heat flow per unit area. The negative sign appears because, in case \mathbf{q} and \mathbf{n} point in the same direction, thermal energy is leaving the volume, hence reducing the thermal energy contained in that volume. In order to arrive at a differential equation, we apply once more Reynolds transport theorem on the left-hand side with $\psi = \rho c_p T$ and Gaussian's divergence theorem on the right-hand side to a subset $\omega(t) \subset \Omega(t)$, which yields

$$\begin{aligned} \frac{d}{dt} \int_{\omega(t)} \rho c_p T \, d\mathbf{x} &= - \int_{\partial\omega(t)} \mathbf{q} \cdot \mathbf{n} \, dS(\mathbf{x}) \\ \Leftrightarrow \int_{\omega(t)} (\partial_t(\rho c_p T) + \operatorname{div}(\rho c_p T \mathbf{u})) \, d\mathbf{x} &= - \int_{\omega(t)} \operatorname{div} \mathbf{q} \, d\mathbf{x}. \end{aligned}$$

Subtracting the right-hand side gives us

$$\Leftrightarrow \int_{\omega(t)} (\partial_t(\rho c_p T) + \operatorname{div}(\rho c_p T \mathbf{u}) + \operatorname{div} \mathbf{q}) \, d\mathbf{x} = 0.$$

Since the subset $\omega(t)$ was chosen to be arbitrary (and the integrand as smooth as necessary), the integrand vanishes altogether:

$$\Leftrightarrow \partial_t(\rho c_p T) + \operatorname{div}(\rho c_p T \mathbf{u}) + \operatorname{div} \mathbf{q} = 0.$$

Since we are dealing with an incompressible fluid, ρ is constant and there holds $\operatorname{div} \mathbf{u} = 0$. Together with the heat capacity being constant as well, this leads to

$$\rho c_p (\partial_t T + \mathbf{u} \cdot \nabla T) + \operatorname{div} \mathbf{q} = 0.$$

The heat flux is determined by *heat conduction*, that is, thermal energy moves from regions with a higher temperature to regions with a lower temperature and is described by **Fourier's law**:

$$\mathbf{q} = -\lambda \nabla T. \tag{2.20}$$

The constant of proportionality λ is the **thermal conductivity** and has the dimension [J/(K m s)]. Thus, we obtain the *heat equation* with convection:

$$\begin{aligned} \rho c_p (\partial_t T + \mathbf{u} \cdot \nabla T) - \operatorname{div}(\lambda \nabla T) &= 0 \\ \Leftrightarrow \rho c_p (\partial_t T + \mathbf{u} \cdot \nabla T) - \lambda \Delta T &= 0. \end{aligned}$$

Although we will not use it here, one can divide by ρc_p , yielding

$$\partial_t T - \alpha \Delta T + \mathbf{u} \cdot \nabla T = 0 \tag{2.21}$$

with the **thermal diffusivity** $\alpha = \lambda/(\rho c_p)$. This is the most common representation of the heat equation (with convection) and the formulation that will be used later in

the numerical examples for convection-diffusion equations. Due to the presence of urea particles in the fluid, this equation has to be extended by two terms, leading to its final form (see Hackbusch et al. [10] and Anker et al. [1]):

$$-\lambda\Delta T + \rho c_p(\partial_t T + \mathbf{u} \cdot \nabla T) + \Delta h_{\text{cryst}} H_\ell = \Delta h_{\text{cryst}} F_\ell, \quad (2.22)$$

where

$$H_\ell = 3\rho^d k_V G(c, T) \int_{\ell_{\min}}^{\ell_{\max}} \ell^2 f \, d\ell \quad \text{and} \quad F_\ell = -\rho^d k_V \ell_{\min}^3 B_{\text{nuc}}. \quad (2.23)$$

The first additional term, $\Delta h_{\text{cryst}} H_\ell$, models the decrease of energy due to growth of particles. The second additional term, $\Delta h_{\text{cryst}} F_\ell$, describes the decrease of energy due to nucleation.

Concentration

Now we turn to the equation for the concentration. We start with the amount of substance in a given volume:

$$\int_{\Omega(t)} c(\mathbf{x}, t) \, d\mathbf{x},$$

where $c(\mathbf{x}, t)$ is the concentration of urea particles dispersed in ethanol with the dimension [mol/m³]. The equation is obtained in the same manner as the heat equation: (i) Equating the rate of change of the amount of substance in an arbitrary volume and the mass flux across its boundary; (ii) applying Reynolds transport theorem and Gaussian's divergence theorem; (iii) making use of the arbitrariness of the subset and the incompressibility of ethanol, leading to the following differential equation:

$$\partial_t c + \mathbf{u} \cdot \nabla c + \text{div} \mathbf{j} = 0,$$

where \mathbf{j} [mol/(s m²)] describes the **mass flux**, that is, the local mass flow per unit area. The underlying process is called *diffusion* in which, analogue to the case of heat conduction, mass is flowing from regions with a higher concentration to regions with a lower one. Mathematically it is represented by **Fick's law**:

$$\mathbf{j} = -D\nabla c$$

with the **diffusion coefficient** D which has the dimension [m²/s]. This leads to the convection-diffusion equation

$$\partial_t c - D\Delta c + \mathbf{u} \cdot \nabla c = 0.$$

Much like in the case of the heat equation, it has to be extended because of the presence of the urea particles to the following equation (see Hackbusch et al. [10] and Anker et al. [1]):

$$\partial_t c - D\Delta c + \mathbf{u} \cdot \nabla c + \frac{H_\ell}{m_{\text{mol}}} = -\frac{F_\ell}{m_{\text{mol}}}, \quad (2.24)$$

where the additional terms already appeared in the heat equation and are given by Equation (2.23). The new terms have an analogous meaning compared to the heat equation:

one models the decrease of the concentration (of dissolved urea) due to particle growth since it is used to enlarge the particles. The other also decreases the concentration but in the case of nucleation new particles have been formed out of dissolved urea and therefore is not longer dissolved.

Now the whole system of equations is complete: Namely the Navier-Stokes equations (2.9), the population balance equation (2.19), the extended heat equation (2.22), and the extended diffusion equation (2.24).

2.4 Population Balance System

In this section we want to summarize all equations, state their initial and boundary conditions, and specify the geometry. Lastly, all appearing functions and physical constants, together with dimensions and numerical value or equation reference, are collected in Table 1.

The flow domain is a tubular pipe. The area is denoted by $B_{\frac{1}{2}}$ where the subscript describes the radius. The domain of the internal variable is an open interval bounded by the minimal and maximal diameter of particles. Hence, we have

$$\Omega := \Omega_x = (0, 210) \times B_{\frac{1}{2}} [\text{cm}^3], \quad \Omega_\ell = (\ell_{\min}, \ell_{\max}) [\text{cm}].$$

The boundary Γ of Ω consists of a union of the inlet boundary Γ_{in} , the outlet boundary Γ_{out} , and the walls Γ_{wall} and are defined as follows

$$\Gamma_{\text{in}} = \{0\} \times B_{\frac{1}{2}}, \quad \Gamma_{\text{out}} = 210 \times B_{\frac{1}{2}}, \quad \Gamma_{\text{wall}} = \Gamma \setminus (\Gamma_{\text{in}} \cup \Gamma_{\text{out}}).$$

First, we derived the Navier-Stokes equations:

$$\begin{aligned} \operatorname{div} \mathbf{u} &= 0 \\ \rho \partial_t \mathbf{u} - \mu \Delta \mathbf{u} + \rho \mathbf{u} \cdot \nabla \mathbf{u} + \nabla p &= \rho \mathbf{g} \end{aligned}$$

The boundary condition on the outlet is the so-called do-nothing condition

$$(\mu \nabla \mathbf{u} - p \boldsymbol{\delta}) \cdot \mathbf{n} = \mathbf{0}, \quad \text{on } \Gamma_{\text{out}}, \quad (2.25)$$

which is a common choice in numerical simulations. A boundary condition at the outlet is not known from experiments and it is unclear how well this unknown boundary condition corresponds to the one given above. Because of that, the length of the computational domain was chosen larger than the length of the pipe used in the experiments (210 cm instead of 200 cm) such that a possible slight incorrectness of the chosen outflow boundary condition does not alter the computational results in the region corresponding to the outlet of the pipe. Since we are dealing with a viscous fluid we employ the no-slip boundary condition at the wall:

$$\mathbf{u}(\mathbf{x}) = \mathbf{0} \quad \text{on } \Gamma_{\text{wall}}. \quad (2.26)$$

Next, we derived the population balance equation:

$$\begin{aligned} \partial_t f + \mathbf{u} \cdot \nabla f + G(c, T) \partial_\ell f &= \frac{3k_V \ell^2}{2} \int_0^V K(V - V', V') f_V(V - V') f_V(V') dV' \\ &\quad - 3k_V \ell^2 f_V(V) \int_0^{V_{\max}} K(V, V') f_V(V') dV'. \end{aligned}$$

The initial condition is given by

$$f(\mathbf{x}, \ell, 0) = 0, \quad \mathbf{x} \in \Omega, \ell \in (\ell_{\min}, \ell_{\max}),$$

meaning that at first there are no particles in the flow domain. The idea of a one-dimensional domain where a fluid flows from left to right can be adopted to the interval $(\ell_{\min}, \ell_{\max})$: As the internal variable ℓ increases, particles get larger; they grow. That means that particle growth can be viewed as ‘flow’ in the abstract space of the internal coordinate. Similarly, as fluid may enter the flow domain, particles may enter the abstract domain. This is exactly the case of nucleation: New particles are created at the ‘inlet’ $\ell = \ell_{\min}$ if the concentration is sufficiently large. This is given by

$$f(\mathbf{x}, \ell_{\min}, t) = \frac{B_{\text{nuc}}}{G(c, T)}, \quad \mathbf{x} \in \Omega, t \in [0, t_{\text{end}}), \text{ if } G(c, T) > 0, \quad (2.27)$$

with the **nucleation rate** B_{nuc} being defined by (see Anker et al. [1])

$$B_{\text{nuc}} = \begin{cases} \alpha_{\text{nuc}} \exp\left(\frac{-\beta_{\text{nuc}}}{\ln^2(c/c_{\text{sat}}(T))}\right), & \text{if } c > c_{\text{sat}}(T), \\ 0, & \text{else,} \end{cases}$$

where $\alpha_{\text{nuc}} = 10^8$ is the nucleation constant and $\beta_{\text{nuc}} = 1.666667 \cdot 10^{-4}$ a model constant. The inlet condition for the particle inflow has the following form

$$f(\mathbf{x}, \ell, t) = \begin{cases} f_{\text{in}}(\ell), & \text{if } t \leq t_{\text{inj}}, \mathbf{x} \in \Gamma_{\text{in}}, \\ 0, & \text{if } t > t_{\text{inj}}, \mathbf{x} \in \Gamma_{\text{in}}. \end{cases} \quad (2.28)$$

It is based on a space-time-averaged inlet condition from experiments pursued by Borchert and Sundmacher [4] while the derivation follows Hackbusch et al. [10]. In the experiments, the particles were injected within a time interval $[0, t_{\text{inj}}]$ into the flow domain with a flow rate \dot{V} [m/s]. The distribution of the number of particles per diameter $f_{\text{seed}}(\ell)$ [1/m] was measured, which represents the number of all particles with a specific length and can be understood as the particle size distribution integrated with respect to the spatial coordinates. One can show the following relationship (see Hackbusch et al. [10]):

$$f_{\text{in}}(\ell) = \frac{6 \cdot 10^7}{t_{\text{inj}} \dot{V}} f_{\text{seed}}(\ell),$$

where the injection time t_{inj} was set to 5 s. Following the work of Anker et al. [1], we use a continuous entering of particles into the domain where finally a steady-state is reached. Accordingly, t_{inj} is set to 300:

$$f_{\text{in}}(\ell) = \frac{6 \cdot 10^7}{300 \dot{V}} f_{\text{seed}}(\ell). \quad (2.29)$$

In the population balance equation two additional phase variables appear. One of them is the temperature, for which we have the following equation:

$$-\lambda \Delta T + \rho c_p (\partial_t T + \mathbf{u} \cdot \nabla T) + 3 \Delta h_{\text{cryst}} \rho^d k_V G(c, T) \int_{\ell_{\min}}^{\ell_{\max}} \ell^2 f \, d\ell = -\Delta h_{\text{cryst}} \rho^d k_V \ell_{\min}^3 B_{\text{nuc}}.$$

The initial and boundary conditions are known from the experiments:

$$\begin{aligned}
T(\mathbf{x}, t) &= T_{\text{in}} & \mathbf{x} \in \Gamma_{\text{in}}, t \in [0, t_{\text{end}}), \\
\nabla T(\mathbf{x}, t) \cdot \mathbf{n} &= 0 & \mathbf{x} \in \Gamma_{\text{out}}, t \in [0, t_{\text{end}}), \\
T(\mathbf{x}, t) &= T_{\text{wall}} & \mathbf{x} \in \Gamma_{\text{wall}}, t \in [0, t_{\text{end}}), \\
T(\mathbf{x}, 0) &= T_{\text{in}} & \mathbf{x} \in \Omega,
\end{aligned}$$

with $T_{\text{in}} = 301.15$ K and $T_{\text{wall}} = 291.15$ K. The initial condition is prescribed by solving the stationary equation without the coupling term to the PSD. Lastly, we have the equation for the concentration of urea in ethanol

$$\partial_t c - D\Delta c + \mathbf{u} \cdot \nabla c + \frac{3\rho^d k_V G(c, T)}{m_{\text{mol}}} \int_{\ell_{\text{min}}}^{\ell_{\text{max}}} \ell^2 f \, d\ell = -\frac{\rho^d k_V \ell_{\text{min}}^3 B_{\text{nuc}}}{m_{\text{mol}}}.$$

The corresponding initial and boundary conditions are

$$\begin{aligned}
c(\mathbf{x}, t) &= c_{\text{sat}}(T_{\text{in}}) & \mathbf{x} \in \Gamma_{\text{in}}, t \in [0, t_{\text{end}}), \\
\nabla c(\mathbf{x}, t) \cdot \mathbf{n} &= 0 & \mathbf{x} \in \Gamma_{\text{out}} \cup \Gamma_{\text{wall}}, t \in [0, t_{\text{end}}), \\
c(\mathbf{x}, 0) &= c_{\text{sat}}(T_{\text{in}}) & \mathbf{x} \in \Omega.
\end{aligned}$$

Table 1: All appearing variables and constants in the system

entity	dimension	description	value/equation reference
$\mathbf{u}(\mathbf{x}, t)$	m/s	velocity	Equation (2.9)
ρ	kg/m ³	density of ethanol	789
$p(\mathbf{x}, t)$	N/m ²	pressure	Equation (2.9)
μ	kg/(m s)	dynamic viscosity of ethanol	$1.074 \cdot 10^{-3}$
$f(\mathbf{x}, \ell, t)$	1/m ⁴	average number density	Equation (2.19)
ℓ	m	diameter of urea particle (inner variable)	–
$G(c, T)$	m/s	growth rate	Equation (2.17)
$K(V, V')$	1/m ¹²	aggregation kernel	Equation (2.11)
k_V	1	volume shape factor	$\pi/6$
ℓ_{min}	m	minimal particle diameter	$2.5 \cdot 10^{-6}$
ℓ_{max}	m	maximal particle diameter	$5 \cdot 10^{-3}$
f_{in}	1/m ⁴	number density at the inlet	Equation (2.29)
$T(\mathbf{x}, t)$	K	temperature	Equation (2.22)
λ	W/(K m)	thermal conductivity	0.167
c_p	J/(kg K)	heat capacity	2441.3
Δh_{cryst}	J/kg	enthalpy change of solution	$2.1645 \cdot 10^5$
ρ^d	kg/m ³	density of urea	1323
B_{nuc}	1/(m ³ s)	nucleation rate	10^8
m_{mol}	kg/mol	molar mass	$60.06 \cdot 10^{-3}$
T_{in}	K	temperature at the inlet	301.15
T_{wall}	K	temperature of the wall	291.15
$c(\mathbf{x}, t)$	mol/m ³	concentration	Equation (2.24)
D	m ² /s	diffusion coefficient of urea in ethanol	$1.35 \cdot 10^{-9}$
c_{sat}	mol/m ³	saturation concentration	Equation (2.18)

2.5 Nondimensionalization

Nondimensionalization is used for several reasons.

The first being to identify characteristic variables of the system under consideration. With their aid systems which may differ in size can be compared when these variables coincide. This quality is used, for instance, in wind tunnels: The models of cars and airplanes are much smaller (and therefore much cheaper) than actual ones, but the experiments will have the same Reynolds numbers (to be defined subsequently), that flows around real cars and planes have. Thus, results from wind tunnel experiments can be used to judge car design. Another reason is to reduce the number of entities necessary to describe the system. Since the variables are linked with one another, one can describe important features of the system with lesser variables than the formulation in dimensional variables. More information can be found, for instance, in Howison [11], Chapter 3. Another reason is the necessity for numerical computations. To this end reference values are defined, see Table 2.

Table 2: Reference values for the nondimensionalization.

reference variable	value, dimension	description
X_∞	0.01 m	reference length of the spatial domain
ℓ_∞	$5 \cdot 10^{-3}$ m	reference length of the particle diameter
U_∞	0.01 m/s	reference velocity
c_∞	10^3 mol/m ³	reference concentration
T_∞	1 K	reference temperature
f_∞	10^{13} 1/m ⁴	reference number density
t_∞	$X_\infty/U_\infty = 1$ s	reference time
p_∞	ρU_∞^2	reference pressure
g_∞	$U_\infty^2/X_\infty = 0.01$ m ² /s	reference acceleration

With these reference values we define the following dimensionless variables in which the variables with a prime represent the dimensionless entity and the ones without represent the entities already known.

$$\left. \begin{aligned} \mathbf{x}' &= \frac{\mathbf{x}}{X_\infty}, & \ell' &= \frac{\ell}{\ell_\infty}, & t' &= \frac{t}{t_\infty}, & \ell'_{\min} &= \frac{\ell_{\min}}{\ell_\infty}, & \ell'_{\max} &= \frac{\ell_{\max}}{\ell_\infty}, \\ \mathbf{u}' &= \frac{\mathbf{u}}{U_\infty}, & T' &= \frac{T}{T_\infty}, & c' &= \frac{c}{c_\infty}, & f' &= \frac{f}{f_\infty}, & p' &= \frac{p}{p_\infty}, \\ \text{Re} &= \frac{X_\infty U_\infty}{\nu}, & \text{Pe}_c &= \frac{X_\infty U_\infty}{D_c}, & \text{Pe}_T &= \frac{X_\infty U_\infty c_p \rho}{\lambda}. \end{aligned} \right\} \quad (2.30)$$

The last three variables are the **Reynolds number** and the **Péclet number** for diffusion and heat conduction, respectively. The Reynolds number, Re , is defined as the ratio of inertial forces to viscous forces, the Péclet number, Pe_c , as the ratio of convective to diffusive transport of particles, and the Péclet number, Pe_T , as the ratio of convective to diffusive heat transfer. Hence, these variables show which of the physical phenomena dominate.

Any function can be expressed in terms of dimensional variables or nondimensional variables. Consequently, there are two types of derivatives, e.g., for the partial derivative

with respect to time:

$$\frac{\partial f(t)}{\partial t}, \quad \frac{\partial f(t')}{\partial t'}.$$

Using the chain rule we can link both types of derivatives:

$$\partial_t f(t') = \frac{\partial}{\partial t} f(t') = \frac{\partial f(t')}{\partial t'} \frac{dt'}{dt} = \frac{\partial f(t')}{\partial t'} \frac{1}{t_\infty} = \frac{1}{t_\infty} \partial_{t'} f(t').$$

Analogously we get

$$\nabla f(\mathbf{x}') = \frac{1}{X_\infty} \nabla' f(\mathbf{x}'), \quad \Delta f(\mathbf{x}') = \frac{1}{X_\infty^2} \Delta' f(\mathbf{x}'), \quad \partial_\ell f(\ell') = \frac{1}{\ell_\infty} \partial_{\ell'} f(\ell'),$$

where ∇' and Δ' represent the gradient and Laplacian with respect to \mathbf{x}' . Next, we replace the dimensional variables and derivatives by the nondimensional ones and insert the definitions of U_∞ , p_∞ , and g_∞ . For instance, the second equation of the Navier-Stokes equations (2.9) transforms to:

$$\begin{aligned} \frac{U_\infty^2}{X_\infty} \partial_{t'} \mathbf{u}' - \frac{\nu U_\infty}{X_\infty^2} \Delta' \mathbf{u}' + \frac{U_\infty^2}{X_\infty} \mathbf{u}' \cdot \nabla' \mathbf{u}' + \frac{U_\infty^2}{X_\infty} \nabla' p' &= \frac{U_\infty^2}{X_\infty} \mathbf{g}'. \\ \Leftrightarrow \partial_{t'} \mathbf{u}' - \frac{\nu}{X_\infty U_\infty} \Delta' \mathbf{u}' + \mathbf{u}' \cdot \nabla' \mathbf{u}' + \nabla' p' &= \mathbf{g}'. \end{aligned}$$

Recalling the definition of the Reynolds number, Re , one gets

$$\Leftrightarrow \partial_{t'} \mathbf{u}' - \frac{1}{\text{Re}} \Delta' \mathbf{u}' + \mathbf{u}' \cdot \nabla' \mathbf{u}' + \nabla' p' = \mathbf{g}'.$$

In fluid mechanics, the Reynolds number is of great importance because it indicates whether a flow is laminar or turbulent. For pipes in general, flows with a Reynolds number less than 2300 are considered to be laminar, see Schade et al. [28, chapter 5.1]. The Reynolds number used in the Navier-Stokes equations above is defined by the dimensionless reference values, but a better impression of the flow is given if one incorporates the actual fluid velocity at the inlet of the pipe. For the flow considered in this work we have approximately $\text{Re} = 331$ and, therefore, we are dealing with a laminar flow, which will eventually reach a steady state. Hence, it is justified to assume a fully developed flow field, especially since this was the case in the experiments. This leads to the stationary Navier-Stokes equations in nondimensional form:

$$\begin{aligned} \text{div } \mathbf{u} &= 0, \\ -\frac{1}{\text{Re}} \Delta \mathbf{u} + \mathbf{u} \cdot \nabla \mathbf{u} + \nabla p &= \mathbf{g}, \end{aligned} \tag{2.31}$$

where we, following common practice after nondimensionalization, dropped the primes of the nondimensionalized variables and derivatives. The no-slip boundary condition does not change its form after nondimensionalization since the (nondimensionalized) velocity has to equal zero on the wall. For the boundary condition (2.25) we get

$$\left(\frac{\mu U_\infty}{X_\infty} \nabla \mathbf{u} - \rho U_\infty p \boldsymbol{\delta} \right) \cdot \mathbf{n} = \mathbf{0}, \quad \text{on } \Gamma_{\text{out}}.$$

Adopting this methodology to the other equations yields

$$\partial_t f + \mathbf{u} \cdot f + \frac{X_\infty}{U_\infty \ell_\infty} G(c, T) \partial_\ell f = \frac{X_\infty}{U_\infty f_\infty} (A^+[f] + A^-[f]), \quad (2.32)$$

$$\partial_t T - \frac{1}{\text{Pe}_T} \Delta T + \mathbf{u} \cdot \nabla T + H_\ell^T = f_\ell^T, \quad (2.33)$$

$$\partial_t c - \frac{1}{\text{Pe}_c} \Delta c + \mathbf{u} \cdot \nabla c + H_\ell^c = f_\ell^c, \quad (2.34)$$

with

$$\begin{aligned} H_\ell^c &= \frac{X_\infty \ell_\infty^3 f_\infty}{U_\infty c_\infty} \cdot \frac{3\rho^d k_V}{m_{\text{mol}}} G(c, T) \int_{\ell_{\min}}^{\ell_{\max}} \ell^2 f \, d\ell, & f_\ell^c &= -\frac{X_\infty \ell_\infty^3}{U_\infty c_\infty} \cdot \frac{\rho^d k_V \ell_{\min}^3 B_{\text{nuc}}}{m_{\text{mol}}}, \\ H_\ell^T &= \frac{X_\infty \ell_\infty^3 f_\infty}{U_\infty T_\infty} \cdot \frac{3\rho^d k_V \Delta h_{\text{cryst}}}{c_p \rho} G(c, T) \int_{\ell_{\min}}^{\ell_{\max}} \ell^2 f \, d\ell, & f_\ell^T &= -\frac{X_\infty \ell_\infty^3}{U_\infty T_\infty} \cdot \frac{\rho^d k_V \ell_{\min}^3 B_{\text{nuc}} \Delta h_{\text{cryst}}}{c_p \rho}. \end{aligned} \quad (2.35)$$

Note that some of the constants are still dimensional, namely A , ρ^d , m_{mol} , $G(c, T)$, B_{nuc} , c_p , ρ , Δh_{cryst} . One could define corresponding reference values for any of these constants and proceed as done above. However, all the equations are already in dimensionless form and furthermore, one would express the new reference values by means of the old ones and arrive at a similar result. It is a little inconsistent since primed variables were introduced to distinguish those that are dimensional from those that are nondimensional, but the detailed derivation does not differ much from the one used for the Navier-Stokes equations. The initial and boundary conditions are gained in the same manner. In view of the next section, we omit them here and state them at the end of the chapter in their final formulation.

2.6 Cylindrical coordinates

So far we modeled all processes, collected the resulting partial differential equations in a population balance system and nondimensionalized them, leading to equations (2.31) - (2.34). In this last section we want to exploit certain properties of the geometrical domain, namely a pipe, or in other words, a cylinder. Hence cylindrical coordinates seem to be more appropriate to describe the system. They are given by the following transformation

$$\begin{aligned} \Psi : \Omega_c &:= (0, 0.5) \times (0, 2\varphi) \times (0, 210) \rightarrow B_{\frac{1}{2}} \times (0, 210) =: \Omega_x, \\ (r, \varphi, z) &\mapsto (x, y, z) = (r \cos(\varphi), r \sin(\varphi), z), \end{aligned}$$

where Ω_x and Ω_c describe the same physical domain, namely the pipe, but are expressed in different coordinates. The transformation from the Cartesian to the cylindrical coordinate system is performed by means of integration by substitution for multiple variables. For a scalar function f there holds (see Königsberger [19, chapter 9] for a precise definition)

$$\begin{aligned} \int_{\Omega_x} f(x, y, z) \, d(x, y, z) &= \int_{\Omega_c} f(\Psi(r, \varphi, z)) |\det D\Psi(r, \varphi, z)| \, d(r, \varphi, z) \\ &= \int_{\Omega_c} \tilde{f}(r, \varphi, z) r \, d(r, \varphi, z). \end{aligned} \quad (2.36)$$

The notation $d(x, y, z)$ and $d(r, \varphi, z)$ implies that the integration is performed in the corresponding three-dimensional domain (as opposed to three iterated integrals) and $\tilde{f} = f \circ \Psi$ is the function expressed in cylindrical coordinates. Furthermore, $D\Psi$ is the Jacobian matrix of the transformation and $|\det D\Psi(r, \varphi, z)|$ the absolute value of its determinant. A simple calculation yields $|\det D\Psi(r, \varphi, z)| = r$.

Moreover, the derivatives have to be transformed as well. To this end we use the basis vectors of both coordinate systems, namely $(\mathbf{e}_x, \mathbf{e}_y, \mathbf{e}_z)$ and $(\mathbf{e}_r, \mathbf{e}_\varphi, \mathbf{e}_z)$:

$$\mathbf{e}_x = \begin{pmatrix} 1 \\ 0 \\ 0 \end{pmatrix}, \mathbf{e}_y = \begin{pmatrix} 0 \\ 1 \\ 0 \end{pmatrix}, \mathbf{e}_z = \begin{pmatrix} 0 \\ 0 \\ 1 \end{pmatrix}, \quad \mathbf{e}_r = \begin{pmatrix} \cos(\varphi) \\ \sin(\varphi) \\ 0 \end{pmatrix}, \mathbf{e}_\varphi = \begin{pmatrix} -\sin(\varphi) \\ \cos(\varphi) \\ 0 \end{pmatrix}, \mathbf{e}_z = \begin{pmatrix} 0 \\ 0 \\ 1 \end{pmatrix}.$$

With these relations one can transform the basis vectors from one system into the other. Hence, we get

$$\begin{aligned} \mathbf{e}_x &= \cos(\varphi)\mathbf{e}_r - \sin(\varphi)\mathbf{e}_\varphi, \\ \mathbf{e}_y &= \sin(\varphi)\mathbf{e}_r + \cos(\varphi)\mathbf{e}_\varphi. \end{aligned}$$

One can show that the partial derivatives transform in the following way:

$$\begin{aligned} \partial_x &= \cos(\varphi)\partial_r - \frac{\sin(\varphi)}{r}\partial_\varphi, \\ \partial_y &= \sin(\varphi)\partial_r + \frac{\cos(\varphi)}{r}\partial_\varphi. \end{aligned}$$

The partial derivative with respect to z does not change since this coordinate is the same in both coordinate systems. Note that not all basis vectors of the cylindrical coordinate system are constant; the dependency on φ has to be considered in order to transform the differential operators correctly. It holds

$$\partial_\varphi \mathbf{e}_r = \mathbf{e}_\varphi, \quad \partial_\varphi \mathbf{e}_\varphi = -\mathbf{e}_r. \quad (2.37)$$

Now we are able to transform the gradient by using its representation as a vector:

$$\begin{aligned} \nabla &= \mathbf{e}_x \partial_x + \mathbf{e}_y \partial_y + \mathbf{e}_z \partial_z \\ &= (\cos(\varphi)\mathbf{e}_r - \sin(\varphi)\mathbf{e}_\varphi) \left(\cos(\varphi)\partial_r - \frac{\sin(\varphi)}{r}\partial_\varphi \right) \\ &\quad + (\sin(\varphi)\mathbf{e}_r + \cos(\varphi)\mathbf{e}_\varphi) \left(\sin(\varphi)\partial_r + \frac{\cos(\varphi)}{r}\partial_\varphi \right) + \mathbf{e}_z \partial_z. \end{aligned}$$

Multiplying out and using elementary relations of trigonometrical functions yields the gradient in cylindrical coordinates

$$\nabla = \mathbf{e}_r \partial_r + \frac{1}{r} \mathbf{e}_\varphi \partial_\varphi + \mathbf{e}_z \partial_z. \quad (2.38)$$

With this identity one can also express the divergence in cylindrical coordinates if one uses its notation as a scalar product of the gradient vector and a vector field $\tilde{\mathbf{u}} = u_r \mathbf{e}_r + u_\varphi \mathbf{e}_\varphi + u_z \mathbf{e}_z$:

$$\operatorname{div} \tilde{\mathbf{u}} = \nabla \cdot \mathbf{u} = (\mathbf{e}_r \partial_r + \frac{1}{r} \mathbf{e}_\varphi \partial_\varphi + \mathbf{e}_z \partial_z) \cdot (u_r \mathbf{e}_r + u_\varphi \mathbf{e}_\varphi + u_z \mathbf{e}_z).$$

With Equation (2.37) and the orthonormality of the basis one arrives at

$$\operatorname{div} \tilde{\mathbf{u}} = \partial_r u_r + \frac{1}{r} u_r + \frac{1}{r} \partial_\varphi u_\varphi + \partial_z u_z.$$

The Laplacian is then given by

$$\begin{aligned} \Delta &= \nabla \cdot \nabla \\ \Delta &= (\mathbf{e}_r \partial_r + \frac{1}{r} \mathbf{e}_\varphi \partial_\varphi + \mathbf{e}_z \partial_z) \cdot (\mathbf{e}_r \partial_r + \frac{1}{r} \mathbf{e}_\varphi \partial_\varphi + \mathbf{e}_z \partial_z) \\ \Delta &= \partial_r^2 + \frac{1}{r} \partial_r + \frac{1}{r^2} \partial_\varphi^2 + \partial_z^2. \end{aligned} \tag{2.39}$$

Now we are able to transform a scalar equation like Equation (2.33) for the temperature. First we integrate it over the domain of the pipe and apply the transformation (2.36)

$$\begin{aligned} 0 &= \int_{B_{\frac{1}{2}} \times (0, 210)} \left(\partial_t T - \frac{1}{\operatorname{Pe}_T} \Delta T + \mathbf{u} \cdot \nabla T + H_\ell^T - f_\ell^T \right) d(x, y, z) \\ &= \int_{(0, \frac{1}{2}) \times (0, 2\pi) \times (0, 210)} \left(\partial_t \tilde{T} - \frac{1}{\operatorname{Pe}_T} \Delta \tilde{T} + \tilde{\mathbf{u}} \cdot \nabla \tilde{T} + \tilde{H}_\ell^T - \tilde{f}_\ell^T \right) r d(r, \varphi, z), \end{aligned}$$

where the tildes indicate functions expressed in cylindrical coordinates. Note that, for instance, \tilde{H}_ℓ^T , defined in Equation (2.35), depends on c , T , and f , but as there is no differential operator involved it can be easily transformed. Even the integration of f with respect to the internal coordinate does not change that because the integration takes place in a different domain than is being transformed here. With equations (2.38) and (2.39) we get

$$\begin{aligned} 0 &= \int_{(0, \frac{1}{2}) \times (0, 2\pi) \times (0, 210)} \left(\partial_t \tilde{T} - \frac{1}{\operatorname{Pe}_T} \left(\partial_r^2 \tilde{T} + \frac{1}{r} \partial_r \tilde{T} + \frac{1}{r^2} \partial_\varphi^2 \tilde{T} + \partial_z^2 \tilde{T} \right) \right. \\ &\quad \left. + u_r \partial_r \tilde{T} + \frac{u_\varphi}{r} \partial_\varphi \tilde{T} + u_z \partial_z \tilde{T} + \tilde{H}_\ell^T - \tilde{f}_\ell^T \right) r d(r, \varphi, z). \end{aligned}$$

Then we split the integral into three iterated integrals by Fubini's theorem (see Königsberger [19, chapter 8.5]):

$$\begin{aligned} 0 &= \int_{(0, \frac{1}{2})} \int_{(0, 2\pi)} \int_{(0, 210)} \left(\partial_t \tilde{T} - \frac{1}{\operatorname{Pe}_T} \left(\partial_r^2 \tilde{T} + \frac{1}{r} \partial_r \tilde{T} + \frac{1}{r^2} \partial_\varphi^2 \tilde{T} + \partial_z^2 \tilde{T} \right) \right. \\ &\quad \left. + u_r \partial_r \tilde{T} + \frac{u_\varphi}{r} \partial_\varphi \tilde{T} + u_z \partial_z \tilde{T} + \tilde{H}_\ell^T - \tilde{f}_\ell^T \right) r dz d\varphi dr. \end{aligned}$$

Now we want to make the following assumption with far-reaching consequences: Any function is independent of φ and the φ -component of any vector field is identically zero. This assumption is justified because the domain is a cylinder and therefore, has rotational symmetry about the z -axis; the flow has a preferred direction and is laminar as we concluded in the previous section. The immediate consequence is $\partial_\varphi \tilde{T} = \partial_\varphi^2 = u_\varphi = 0$. This simplifies the integral considerably because it reduces the dimension by 1:

$$0 = 2\pi \int_{(0, \frac{1}{2})} \int_{(0, 210)} \left(\partial_t \tilde{T} - \frac{1}{\operatorname{Pe}_T} \left(\partial_r^2 \tilde{T} + \frac{1}{r} \partial_r \tilde{T} + \partial_z^2 \tilde{T} \right) + u_r \partial_r \tilde{T} + u_z \partial_z \tilde{T} + \tilde{H}_\ell^T - \tilde{f}_\ell^T \right) r dz dr.$$

Now we argue again that the integrand has to vanish equally if the integral is zero and the integrand continuous, leading to

$$\partial_t \tilde{T} - \frac{1}{\text{Pe}_T} \left(\partial_r^2 \tilde{T} + \frac{1}{r} \partial_r \tilde{T} + \partial_z^2 \tilde{T} \right) + u_r \partial_r \tilde{T} + u_z \partial_z \tilde{T} + \tilde{H}_\ell^T = \tilde{f}_\ell^T.$$

Applying the same procedure to equations (2.32) and (2.34) yields analogous results and will be given at the end of the section. The transformation of the Navier-Stokes equations is somewhat more complicated. It requires the formulas for the gradient and Laplacian of a vector field whose derivation is quite lengthy and can be found, also for general curvilinear coordinates, in Müller [23]. The (stationary) Navier-Stokes equations in cylindrical coordinates are (see Schade et al. [28, chapter 8.3] and Müller [23, chapter 7.4])

$$\begin{aligned} & \partial_r u_r + \frac{u_r}{r} + \frac{1}{u_r} \partial_\varphi u_\varphi + \partial_z u_z = 0, \\ & -\frac{1}{\text{Re}} \left(\partial_r^2 u_r + \frac{1}{r} \partial_r u_r - \frac{u_r}{r^2} + \frac{1}{r^2} \partial_\varphi^2 u_r + \partial_z^2 u_r - \frac{2}{r^2} \partial_\varphi u_\varphi \right) \\ & \quad + u_r \partial_r u_r + \frac{u_\varphi}{r} \partial_\varphi u_r + u_z \partial_z u_r - \frac{u_\varphi^2}{r} + \partial_r \tilde{p} = g_r, \\ & -\frac{1}{\text{Re}} \left(\partial_r^2 u_\varphi + \frac{1}{r} \partial_r u_\varphi - \frac{u_\varphi}{r^2} + \frac{1}{r^2} \partial_\varphi^2 u_\varphi + \partial_z^2 u_\varphi + \frac{2}{r^2} \partial_\varphi u_r \right) \\ & \quad + u_r \partial_r u_\varphi + \frac{u_\varphi}{r} \partial_\varphi u_\varphi + u_z \partial_z u_\varphi + \frac{u_r u_\varphi}{r} + \frac{1}{r} \partial_\varphi \tilde{p} = g_\varphi, \\ & -\frac{1}{\text{Re}} \left(\partial_r^2 u_z + \frac{1}{r} \partial_r u_z + \frac{1}{r^2} \partial_\varphi^2 u_z + \partial_z^2 u_z \right) \\ & \quad + u_r \partial_r u_z + \frac{u_\varphi}{r} \partial_\varphi u_z + u_z \partial_z u_z + \partial_z \tilde{p} = g_z. \end{aligned} \tag{2.40}$$

Here the consequences of the assumption made above are even greater: The second equation of the impulse balance vanishes completely. If one sets all summands containing u_φ or the partial derivative with respect to φ to zero, one obtains for the remaining equations

$$\begin{aligned} & \partial_r u_r + \frac{u_r}{r} + \partial_z u_z = 0, \\ & -\frac{1}{\text{Re}} \left(\partial_r^2 u_r + \frac{1}{r} \partial_r u_r - \frac{u_r}{r^2} + \partial_z^2 u_r \right) + u_r \partial_r u_r + u_z \partial_z u_r + \partial_r \tilde{p} = g_r, \\ & -\frac{1}{\text{Re}} \left(\partial_r^2 u_z + \frac{1}{r} \partial_r u_z + \partial_z^2 u_z \right) + u_r \partial_r u_z + u_z \partial_z u_z + \partial_z \tilde{p} = g_z. \end{aligned}$$

Following Schade et al. [28, chapter 8.4], we make further assumptions based on empirical insights. From a fluid mechanics point of view, it is clear that laminar flow in a pipe is caused by an external, axial pressure gradient. As a result, the fluid flows in axial direction, i.e., in z -direction, but there is no reason why it should have an azimuthal component, i.e., rotation around the z -axis, or a radial component. Consequently, we assume, additionally to u_φ being zero, that also u_r is equal to 0. As a result, the first equation of the impulse balance is fulfilled identically. Similarly, there is no ‘special’ height z , such that the remaining third component of the velocity is independent of it, leading to

$$\begin{aligned} \tilde{u}(r, \varphi, z) &= u_r(r, \varphi, z) \mathbf{e}_r + u_\varphi(r, \varphi, z) \mathbf{e}_\varphi + u_z(r, \varphi, z) \mathbf{e}_z \\ &= u_z(r) \mathbf{e}_z. \end{aligned}$$

These simplifications are due to the specific case we encounter: there are no bends or kinks in the pipe, i.e. it is completely straight. Moreover, it is located horizontally such that the gravitational force plays a comparably small role and will be neglected from now on. The considerations made so far apply also to the pressure gradient: The partial derivatives of the pressure with respect to r and φ are zero and the z -component of the pressure gradient is independent of φ and z , leading to the ansatz:

$$\partial_r \tilde{p} = 0, \quad \partial_\varphi \tilde{p} = 0, \quad \partial_z \tilde{p} = (\partial_z \tilde{p})(r),$$

where the notation indicates that the partial derivative with respect to z is a function that depends only on r . According to the first equation, \tilde{p} does not depend on the radius r . Consequently, the partial derivative of \tilde{p} with respect to z must be independent of r as well such that the pressure is constant:

$$\frac{d\tilde{p}}{dz} = \text{const.}$$

Altogether, the continuity equation and the first two equations of the impulse balance are fulfilled identically, leaving only one equation to solve:

$$\frac{1}{\text{Re}} \left(\frac{d^2 u_z}{dr^2} + \frac{1}{r} \frac{du_z}{dr} \right) = \frac{d\tilde{p}}{dz} = \text{const.}$$

Restating the velocity derivatives as $\frac{1}{r} \frac{d}{dr} \left(r \frac{du_z}{dr} \right)$ and integrating twice leads to

$$\frac{du_z}{dr} = \frac{\text{Re}}{2} \frac{d\tilde{p}}{dz} r.$$

Integrating over (r, R) with $0 < r < R$ and R being the (nondimensional) radius of the tube yields

$$\frac{\text{Re}}{4} \frac{d\tilde{p}}{dz} (R^2 - r^2) = \underbrace{u_z(R)}_{=0} - u_z(r).$$

That the velocity at the boundary of the tube is zero may be explained in two ways: Firstly, mathematically, a function cannot attain more than one value for one argument. Therefore, the velocity of the fluid located directly at the tube wall and the tube wall itself must have the same value: zero. Secondly, physically, it reflects adhesion, i.e. the process of attachment of a substance to the surface of another substance. This fact enters computational fluid dynamics as the so-called *no-slip* boundary condition that we already encountered in chapter 2.4, see Equation (2.26). This yields

$$u_z(r) = \frac{\text{Re} \cdot R^2}{4} \left(-\frac{d\tilde{p}}{dz} \right) \left[1 - \left(\frac{r}{R} \right)^2 \right],$$

with a constant, negative pressure gradient. This velocity distribution is known as the *Hagen-Poiseuille flow*, for which the following relationship between the flow rate \dot{V} and the pressure gradient holds, see Schade et al. [28, chapter 5.1]:

$$\dot{V} = \frac{\pi R^4}{8\mu} \left(-\frac{d\tilde{p}}{dz} \right).$$

We point out that this equation is formulated entirely with dimensional entities as we use it to determine at first the pressure gradient and then the fluid velocity. The nondimensional formulation involves the Reynolds number, which in turn, is based on the fluid velocity. Accordingly, we also need the Hagen-Poiseuille equation in its dimensional form:

$$u_z(r) = \frac{R^2}{4\mu} \left(-\frac{dp}{dx} \right) \left[1 - \left(\frac{r}{R} \right)^2 \right]$$

Note that the last factor (in brackets) is dimensionless, so that the rest must have the dimension of a velocity. Adopting the definition of dimensionless variables, see Equation (2.30), we set $r' = r/X_\infty$ and $R' = R/X_\infty = 0.005\text{m}/0.01\text{m} = 0.5$. Using this and dividing the whole term by the reference velocity U_∞ m/s we obtain:

$$\begin{aligned} u'_z(r') &= \frac{1}{U_\infty} \frac{R^2}{4\mu} \left(-\frac{dp}{dx} \right) \left[1 - \left(\frac{0.01r'}{0.01 \cdot 0.5} \right)^2 \right] \\ \Leftrightarrow u'_z(r') &= 5.09296 \left(\frac{1}{4} - r'^2 \right). \end{aligned} \quad (2.41)$$

Now our model is complete: In the case of a tube with certain assumptions the Navier-Stokes equations simplified greatly such that an analytic solution could be obtained, Equation (2.41). The spatial dimension of the population balance equation for the particle size distribution, as well as the balance laws for the temperature and the concentration were reduced by 1. The computational domain has to be adjusted to the cylindrical coordinate system. Accordingly, we define

$$\begin{aligned} (r, z) &=: \mathbf{x} \in \Omega_{\text{cyl}} := (0, 0.5) \times (0, 210), & \Omega_\ell &= (\ell_{\min}, \ell_{\max}) = (5 \cdot 10^{-4}, 1), \\ \Gamma_{\text{in}} &:= [0, 0.5] \times \{0\}, & \Gamma_{\text{out}} &:= [0, 0.5] \times \{210\}, & \Gamma_{\text{wall}} &:= \{0.5\} \times [0, 210]. \end{aligned} \quad (2.42)$$

The population balance system in its final formulation is given below and is the basis for computational experiments where, much like in the case of nondimensionalization, we drop the tildes for convenience.

$$\left. \begin{aligned} \partial_t f + u_r \partial_r f + u_z \partial_z f + \frac{X_\infty}{U_\infty \ell_\infty} G(c, T) \partial_\ell f \\ &= \frac{X_\infty}{U_\infty f_\infty} (A^+[f] + A^-[f]), & \mathbf{x} \in \Omega_{\text{cyl}}, \ell \in \Omega_\ell, t \in (0, t_{\text{end}}), \\ f(\mathbf{x}, \ell, t) &= \frac{6 \cdot 10^7}{f_\infty t_{\text{end}} V_r} f_{\text{seed}}(\ell), & \mathbf{x} \in \Gamma_{\text{in}}, \ell \in \Omega_\ell, t \in [0, t_{\text{end}}) \\ f(\mathbf{x}, \ell_{\min}, t) &= \frac{B_{\text{nuc}}}{f_\infty G(c, T)}, & \mathbf{x} \in \Omega_{\text{cyl}}, t \in (0, t_{\text{end}}), \text{ if } G(c, T) > 0, \\ f(\mathbf{x}, \ell, 0) &= 0, & \mathbf{x} \in \Omega_{\text{cyl}}, \ell \in \Omega_\ell. \end{aligned} \right\} \quad (2.43)$$

$$\left. \begin{aligned}
& \partial_t T - \frac{1}{\text{Pe}_T} \left(\partial_r^2 T + \frac{1}{r} \partial_r T + \partial_z^2 T \right) \\
& \quad + u_r \partial_r T + u_z \partial_z T + H_\ell^T = f_\ell^T, \quad \mathbf{x} \in \Omega_{\text{cyl}}, t \in (0, t_{\text{end}}), \\
& \quad T(\mathbf{x}, t) = \frac{T_{\text{in}}}{T_\infty}, \quad \mathbf{x} \in \Gamma_{\text{in}}, t \in [0, t_{\text{end}}), \\
& \quad \nabla T(\mathbf{x}, t) \cdot \mathbf{n} = 0, \quad \mathbf{x} \in \Gamma_{\text{out}}, t \in [0, t_{\text{end}}), \\
& \quad T(\mathbf{x}, t) = \frac{T_{\text{wall}}}{T_\infty}, \quad \mathbf{x} \in (0, 210), t \in [0, t_{\text{end}}), \\
& \quad T(\mathbf{x}, 0) = \frac{T_{\text{in}}}{T_\infty}, \quad \mathbf{x} \in \Omega_{\text{cyl}},
\end{aligned} \right\} \quad (2.44)$$

$$\left. \begin{aligned}
& \partial_t c - \frac{1}{\text{Pe}_c} \left(\partial_r^2 c + \frac{1}{r} \partial_r c + \partial_z^2 c \right) \\
& \quad + u_r \partial_r c + u_z \partial_z c + H_\ell^c = f_\ell^c, \quad \mathbf{x} \in \Omega_{\text{cyl}}, t \in (0, t_{\text{end}}), \\
& \quad c(\mathbf{x}, t) = \frac{c_{\text{sat}}(T_{\text{in}})}{c_\infty}, \quad \mathbf{x} \in \Gamma_{\text{in}}, t \in [0, t_{\text{end}}), \\
& \quad c(\mathbf{x}, t) = 0, \quad \mathbf{x} \in \Gamma_{\text{out}} \cup \Gamma_{\text{wall}}, t \in [0, t_{\text{end}}), \\
& \quad c(\mathbf{x}, 0) = \frac{c_{\text{sat}}(T_{\text{in}})}{c_\infty} \quad \mathbf{x} \in \Omega.
\end{aligned} \right\} \quad (2.45)$$

3 The Finite Volume Method

The finite volume method (FVM), like the finite difference method (FDM) and the finite element method (FEM), is a popular method used to solve partial differential equations. The FDM works directly with the differential representation of conservation or balance laws whereas the FEM uses a variational principle to obtain a weak solution. In the derivation of the balance laws one arrives initially at an integral equation and obtains the differential equation only after using the fact that if an integral equals zero, the integrand equals zero almost everywhere inside the domain. Even though the derivation of the finite volume method will start with the differential representation of the balance laws as well, one can think of applying the balance laws directly to a finite volume and, that way, the method has more physical basis and interpretation.

3.1 Preliminaries

The derivation of the finite volume method is taken from [1]. The definitions and theorems are given. For proofs and more details, the reader may refer to this paper.

We start the construction of the finite volume method with an open, bounded, connected, and polygonal domain Ω . Let $\{\mathbf{x}_i\}_{i \in \mathcal{N}} \subset \bar{\Omega}$ be a finite set of points, denoted as **discretization points**, **nodes**, or **vertices**. To each node we associate a convex polygonal domain ω_i , called **finite volume**, containing \mathbf{x}_i in its closure.

Definition 3.1. *The set $\mathcal{V} = \{(\mathbf{x}_i, \omega_i)\}_{i \in \mathcal{N}}$ of pairs of discretization vertices and finite volumes is called a **finite volume partition** of Ω if*

$$\bigcup_{i \in \mathcal{N}} \bar{\omega}_i = \bar{\Omega} \quad \text{and} \quad \omega_i \cap \omega_j = \emptyset \quad \forall i, j \in \mathcal{N}.$$

The **intersection face** is defined by $\gamma_{ij} = \bar{\omega}_i \cap \bar{\omega}_j$. If an intersection face consists of more than one point, the corresponding nodes are called **adjacent** and we introduce the **discretization edge** $\mathbf{h}_{ij} = \mathbf{x}_j - \mathbf{x}_i$. For a given point \mathbf{x}_i we call the set $\mathbf{nb}(i)$ of adjacent nodes **neighborhood**. The sets \mathcal{H} and \mathcal{E} denote all discretization edges and all intersection faces of a finite volume partition, respectively, i.e.,

$$\mathcal{H} = \bigcup_{i \in \mathcal{N}} \bigcup_{j \in \mathbf{nb}(i)} \mathbf{h}_{ij}, \quad \mathcal{E} = \bigcup_{i \in \mathcal{N}} \bigcup_{j \in \mathbf{nb}(i)} \gamma_{ij}.$$

Since all finite volumes are polygonal, all intersection faces between neighbors are flat hyperplanes, and the boundary of a finite volume may be represented as a disjoint union of a finite number of intersection faces:

$$\partial\omega_i = \bigcup_{j \in \mathbf{nb}(i)} \gamma_{ij}.$$

A discretization point \mathbf{x}_i is called a **tentative boundary discretization point** if the intersection of the closure of its finite volume $\bar{\omega}_i$ and the boundary of the domain $\partial\Omega$ consists of more than one point. Again, because of the simple geometry of the finite volumes, this set can be represented as a finite, disjoint union of hyperplanes:

$$\bar{\omega}_i \cap \partial\Omega = \bigcup_{o \in \mathcal{B}(i)} \gamma_o,$$

where $\mathcal{B}(i)$ denotes all intersection faces of node \mathbf{x}_i lying on the boundary.

Definition 3.2. A finite volume partition is called **admissible** if it fulfills the following conditions:

- (i) For two adjacent nodes \mathbf{x}_i and \mathbf{x}_j the intersection face γ_{ij} is orthogonal to the edge \mathbf{h}_{ij} .
- (ii) Each tentative boundary discretization point is located at the boundary $\partial\Omega$.

3.2 An introductory example: The Heat Equation

After the definitions are made, we are now able to discretize partial differential equations. Before we deal with the population balance equation for the particle size distribution, the foregoing shall be illustrated first by the discretization of the heat equation and then by a linear, scalar convection-diffusion-reaction equation.

The heat equation is defined as follows:

$$\begin{aligned} \partial_t u + \operatorname{div}(-\alpha \nabla u) &= 0 \quad \text{in } \Omega \times (0, t_{\text{end}}), \\ \nabla u \cdot \mathbf{n} &= 0 \quad \text{on } \Gamma_N \times (0, t_{\text{end}}], \\ u(\cdot, 0) &= u_0 \quad \text{in } \Omega, \end{aligned} \tag{3.1}$$

where α is the thermal diffusivity, u_0 the initial condition, Γ_N the Neumann boundary and we set $\partial\Omega = \Gamma_N$. Note that this problem is only solvable up to a constant since there are only Neumann boundary conditions given. The aim is, however, to provide an easy access to the discretization techniques, since it may be rather technical later on.

Let $\mathbf{x}_i \in \Omega$ be an arbitrary node in the domain and let the time interval $[0, t_{\text{end}}]$ be partitioned in times $0 = t^0 < t^1 < \dots < t^M = t_{\text{end}}$ with time steps $\tau^n = [t^n, t^{n+1}]$. Assume an admissible finite volume partition and denote $u_i^n = u(\mathbf{x}_i, t^n)$. We start with the integration of (3.1) over ω_i and τ^n and split the sum into two terms:

$$0 = \int_{\tau^n} \int_{\omega_i} \partial_t u \, dx \, dt + \int_{\tau^n} \int_{\omega_i} \operatorname{div}(-\alpha \nabla u) \, dx \, dt.$$

In the first term, we switch the order of integration by Fubini's theorem and use the fundamental theorem of calculus. In the second term, we apply the Gaussian divergence theorem and obtain

$$= \int_{\omega_i} (u^{n+1} - u^n) \, dx + \int_{\tau^n} \int_{\partial\omega_i} -\alpha \nabla u \cdot \mathbf{n}_i \, dS(x) \, dt.$$

Note that no integrals over the Neumann boundary appear since there is only a homogeneous Neumann boundary condition prescribed. As stated above, the boundary of a finite volume can be represented as a finite disjoint union of flat hyperplanes. Hence, the boundary integral can be written as a sum over these hyperplanes:

$$= \int_{\omega_i} (u^{n+1} - u^n) \, dx + \int_{\tau^n} \sum_{j \in \mathbf{nb}(i)} \int_{\gamma_{ij}} -\alpha \underbrace{\nabla u \cdot \mathbf{n}_{ij}}_{= \frac{\partial u}{\partial \mathbf{n}_{ij}}} \, dS(x) \, dt. \tag{3.2}$$

We use the midpoint rule to approximate the first integral where only the value of the function at point \mathbf{x}_i is being used. In the second term the directional derivative is approximated with a central finite difference in the direction of the normal, that is, in the direction of neighbor \mathbf{x}_j . That leads to

$$\approx |\omega_i|(u^{n+1} - u^n) + \int_{\tau^n} \sum_{j \in \text{nb}(i)} \int_{\gamma_{ij}} -\alpha \left(\frac{u_j - u_i}{h_{ij}} \right) dS(x) dt.$$

The remaining integrand does not depend on the location, so it is a constant with respect to the boundary integral. In order to obtain a fully implicit scheme (with respect to time) the functions only at the next time are used. This yields the final discretization:

$$0 = |\omega_i|(u_i^{n+1} - u_i^n) + |\tau^n|k \sum_{j \in \text{nb}(i)} \frac{|\gamma_{ij}|}{h_{ij}} (u_i^{n+1} - u_j^{n+1}). \quad (3.3)$$

Before we proceed with the discretization of the more complex equations, let us take a look at the resulting system of linear equations. The diagonal entries of the stiffness matrix $A = (a_{ij})_{i,j=1}^N$ are determined by the coefficients of u_i^{n+1} ; the off-diagonal entries by the coefficients of u_j^{n+1} . Since this depends on the location of the neighbors in the mesh, one cannot write down the whole matrix, but only the entries, which are given below:

$$a_{ij} = \begin{cases} |\omega_i| + \sum_{l \in \text{nb}(i)} |\tau^n| \alpha \frac{|\gamma_{il}|}{h_{il}} & \text{if } i = j, \\ -|\tau^n| \alpha \frac{|\gamma_{ij}|}{h_{ij}} & \text{if } i \neq j, \mathbf{h}_{ij} \in \mathcal{H}, \\ 0 & \text{else.} \end{cases} \quad (3.4)$$

The matrix $B = (b_{ij})_{i,j=1}^N$ contains the coefficients of u_i^n and is a diagonal matrix:

$$b_{ij} = \begin{cases} |\omega_i| & \text{if } i = j, \\ 0 & \text{else.} \end{cases} \quad (3.5)$$

With these matrices the discretized system can be written in the following way

$$Au^{n+1} - Bu^n = 0. \quad (3.6)$$

To analyze the solvability of the resulting linear system, it is convenient to rewrite it with the matrix $A' := A - B$ as such:

$$\begin{aligned} (A' + B)u^{n+1} - Bu^n &= 0 \\ \Leftrightarrow B^{-1}(A' + B)u^{n+1} &= u^n \\ \Leftrightarrow (B^{-1}A' + I)u^{n+1} &= u^n. \end{aligned}$$

By the definitions of A and B , Equations (3.4) and (3.5) respectively, it follows that the sum of each row of A' is zero (as well as of $B^{-1}A'$), such that the matrix $B^{-1}A' + I$ is strictly diagonally dominant, which implies the unique solvability of the system.

3.3 The convection-diffusion-reaction equation

Now we want to discretize a linear, scalar convection-diffusion-reaction equation. We also assume an inhomogeneous right-hand side as well as inhomogeneous Neumann and

Dirichlet boundary conditions. The problem is defined in detail as follows:

$$\begin{aligned} \partial_t u + \operatorname{div}(-\alpha \nabla u + \mathbf{b}u) + cu &= f && \text{in } \Omega \times (0, t_{\text{end}}), \\ \nabla u \cdot \mathbf{n} &= g && \text{on } \Gamma_N \times (0, t_{\text{end}}], \\ u &= u_D && \text{on } \Gamma_D \times (0, t_{\text{end}}], \\ u(\cdot, 0) &= u_0 && \text{in } \Omega, \end{aligned}$$

where Γ_N is the Neumann boundary, Γ_D is the Dirichlet boundary, $\Gamma_N \cup \Gamma_D = \partial\Omega$, u_0 is the initial condition. The inhomogeneity f describes source and sink terms, α is the diffusivity, \mathbf{b} the fluid velocity and the term cu accounts for the reaction. The functions u_D and g are given functions on the corresponding domains. The coefficients are assumed to be constant.

We start with the same step as above: Integrating over a finite volume ω_i and a time step τ^n where we assume that the corresponding node is located either on the Neumann boundary or inside the domain, that is, $x_i \in \Omega \cup \Gamma_N$. The Dirichlet condition will be incorporated later in a different way.

$$\begin{aligned} \int_{\tau^n} \int_{\omega_i} f \, dx \, dt &= \int_{\tau^n} \int_{\omega_i} (\partial_t u + \operatorname{div}(-\alpha \nabla u + \mathbf{b}u) + cu) \, dx \, dt \\ &= \int_{\omega_i} \int_{\tau^n} \partial_t u \, dt \, dx + \int_{\tau^n} \int_{\omega_i} \operatorname{div}(-\alpha \nabla u + \mathbf{b}u) \, dx \, dt + \int_{\tau^n} \int_{\omega_i} cu \, dx \, dt. \end{aligned}$$

Applying the same theorems as we did above and making use of the simple geometry of a finite volume yields

$$\begin{aligned} &= \int_{\omega_i} (u^{n+1} - u^n) \, dx + \int_{\tau^n} \sum_{j \in \mathbf{nb}(i)} \int_{\gamma_{ij}} (-\alpha \nabla u + \mathbf{b}u) \cdot \mathbf{n}_{ij} \, dS(x) \, dt \\ &\quad + \int_{\tau^n} \sum_{o \in \mathcal{B}(i)} \int_{\gamma_o} (-\alpha \nabla u + \mathbf{b}u) \cdot \mathbf{n}_o \, dS(x) \, dt + \int_{\tau^n} \int_{\omega_i} cu \, dx \, dt. \end{aligned}$$

Here we have to consider the Neumann boundary, because on one hand the boundary condition is not homogeneous but states $\nabla u \cdot \mathbf{n}_o = g(\mathbf{x}, t)$, and on the other hand the convective part would not vanish as it is. This gives us

$$\begin{aligned} &= \int_{\omega_i} (u^{n+1} - u^n) \, dx + \int_{\tau^n} \sum_{j \in \mathbf{nb}(i)} \int_{\gamma_{ij}} (-\alpha \nabla u \cdot \mathbf{n}_{ij} + \mathbf{b}u \cdot \mathbf{n}_{ij}) \, dS(x) \, dt \\ &\quad + \int_{\tau^n} \sum_{o \in \mathcal{B}(i)} \int_{\gamma_o} (u \mathbf{b} \cdot \mathbf{n}_o - \alpha g) \, dS(x) \, dt + \int_{\tau^n} \int_{\omega_i} cu \, dx \, dt. \end{aligned}$$

Note that by the use of the Neumann boundary condition the term is no longer containing the unknown function u . Hence, we subtract it and treat it together with the right-hand

side. This leads to the following equation:

$$\begin{aligned}
\int_{\tau^n} \int_{\omega_i} f \, dx \, dt + \int_{\tau^n} \sum_{o \in \mathcal{B}(i)} \int_{\gamma_o} \alpha g \, dS(x) \, dt = \\
\int_{\omega_i} (u^{n+1} - u^n) \, dx + \int_{\tau^n} \sum_{j \in \mathbf{nb}(i)} \int_{\gamma_{ij}} (-\alpha \nabla u \cdot \mathbf{n}_{ij} + \mathbf{b}u \cdot \mathbf{n}_{ij}) \, dS(x) \, dt \\
+ \int_{\tau^n} \sum_{o \in \mathcal{B}(i)} \int_{\gamma_o} \mathbf{u}\mathbf{b} \cdot \mathbf{n}_o \, dS(x) \, dt + \int_{\tau^n} \int_{\omega_i} cu \, dx \, dt.
\end{aligned} \tag{3.7}$$

For the sake of clarity we treat each summand individually. The first term we approximate by the midpoint rule:

$$\int_{\omega_i} (u^{n+1} - u^n) \, dx \approx |\omega_i| (u^{n+1} - u^n). \tag{3.8}$$

For the convective part of the second term we use a *simple upwind scheme*. This is employed by a function that, based on the sign of the argument, lets us choose either the node \mathbf{x}_i or its neighbor \mathbf{x}_j . More precisely, we define ξ as follows

$$\xi(a) = \begin{cases} a & \text{if } a < 0, \\ 0 & \text{else} \end{cases}$$

and use the following approximation:

$$\mathbf{u}\mathbf{b} \cdot \mathbf{n}_{ij} \approx \frac{1}{h_{ij}} \left(\xi(\mathbf{b} \cdot \mathbf{h}_{ij}) u_j - \xi(-\mathbf{b} \cdot \mathbf{h}_{ij}) u_i \right). \tag{3.9}$$

This way, it is assured that only the node \mathbf{x}_i or its neighbor upstream is chosen but never its downstream neighbor. This is done because the information of the solution originates upstream. If one would use, for instance, a central difference scheme, uncertain information from the downstream direction would be incorporated and leads to strong stability problems, see Roos et al. [26, chapter 2] for a detailed treatment. Hence, we choose a difference scheme in the direction where the information comes from. Using that together with a finite difference scheme for the diffusive term and a fully implicit time scheme for the second term of equation (3.7) leads to:

$$\begin{aligned}
\int_{\tau^n} \sum_{j \in \mathbf{nb}(i)} \int_{\gamma_{ij}} (-\alpha \nabla u \cdot \mathbf{n}_{ij} + \mathbf{b}u \cdot \mathbf{n}_{ij}) \, dS(x) \, dt \\
\approx |\tau^n| \sum_{j \in \mathbf{nb}(i)} \frac{|\gamma_{ij}|}{h_{ij}} \left(\left(\xi(\mathbf{b} \cdot \mathbf{h}_{ij}) - \alpha \right) u_j^{n+1} + \left(\alpha - \xi(-\mathbf{b} \cdot \mathbf{h}_{ij}) \right) u_i^{n+1} \right).
\end{aligned} \tag{3.10}$$

The third term is simply approximated by a fully implicit time scheme and a midpoint rule in space since in an admissible finite volume partition the tentative boundary discretization points are located at the boundary. This gives us:

$$\int_{\tau^n} \sum_{o \in \mathcal{B}(i)} \int_{\gamma_o} \mathbf{u}\mathbf{b} \cdot \mathbf{n}_o \, dS(x) \, dt \approx |\tau^n| \sum_{o \in \mathcal{B}(i)} |\gamma_o| (\mathbf{b} \cdot \mathbf{n}_o) u_i^{n+1}. \tag{3.11}$$

For the last term we use again a fully implicit time scheme and the midpoint rule for the integral in space:

$$\int_{\tau^n} \int_{\omega_i} cu \, dx \, dt \approx |\tau^n| |\omega_i| cu_i^{n+1}. \quad (3.12)$$

Lastly, the right-hand side has to be approximated which is done with a fully implicit time scheme and the midpoint rule for both the finite volume and the intersection face. Adopting the notation of u for f and g , i.e., $f_i^n = f(\mathbf{x}_i, t^n)$ and $g_i^n = g(\mathbf{x}_i, t^n)$, yields:

$$\int_{\tau^n} \int_{\omega_i} f \, dx \, dt + \int_{\tau^n} \sum_{o \in \mathcal{B}(i)} \int_{\gamma_o} \alpha g \, dS(x) \, dt \approx |\tau^n| |\omega_i| f_i^{n+1} + |\tau^n| \sum_{o \in \mathcal{B}(i)} |\gamma_o| \alpha g_i^{n+1}. \quad (3.13)$$

Inserting all approximations, namely Equations (3.8), (3.10), (3.11), (3.12), and (3.13), into Equation (3.7) leads to the final discretization of a scalar, linear convection-diffusion-reaction equation:

$$\begin{aligned} |\tau^n| |\omega_i| f_i^{n+1} + |\tau^n| \sum_{o \in \mathcal{B}(i)} |\gamma_o| \alpha g_i^{n+1} &= |\omega_i| (u^{n+1} - u^n) \\ &+ |\tau^n| \sum_{j \in \mathbf{nb}(i)} \frac{|\gamma_{ij}|}{h_{ij}} \left((\xi(\mathbf{b} \cdot \mathbf{h}_{ij}) - \alpha) u_j^{n+1} + (\alpha - \xi(-\mathbf{b} \cdot \mathbf{h}_{ij})) u_i^{n+1} \right) \\ &+ |\tau^n| \sum_{o \in \mathcal{B}(i)} |\gamma_o| (\mathbf{b} \cdot \mathbf{n}_o) u_i^{n+1} + |\tau^n| |\omega_i| cu_i^{n+1}. \end{aligned} \quad (3.14)$$

Again, this can be summarized in a linear system, $Au^{n+1} - Bu^n = D$, with the following entries:

$$\begin{aligned} a_{ij} &= \begin{cases} |\omega_i| + |\tau^n| \left(\sum_{l \in \mathbf{nb}(i)} \frac{|\gamma_{il}|}{h_{il}} (\alpha - \xi(-\mathbf{b} \cdot \mathbf{h}_{ij})) + |\omega_i| c \right) & \text{if } i = j, \mathbf{x}_i \in \mathring{\Omega}, \\ |\omega_i| + |\tau^n| \left(\sum_{l \in \mathbf{nb}(i)} \frac{|\gamma_{il}|}{h_{il}} (\alpha - \xi(-\mathbf{b} \cdot \mathbf{h}_{ij})) + \sum_{o \in \mathcal{B}(i)} |\gamma_o| (\mathbf{b} \cdot \mathbf{n}_o) + |\omega_i| c \right) & \text{if } i = j, \mathbf{x}_i \in \Gamma_N, \\ |\tau^n| \frac{|\gamma_{ij}|}{h_{ij}} (\xi(\mathbf{b} \cdot \mathbf{h}_{ij}) - \alpha) & \text{if } i \neq j, \mathbf{h}_{ij} \in \mathcal{H}, \\ 1 & \text{if } i = j, \mathbf{x}_i \in \Gamma_D, \\ 0 & \text{else,} \end{cases} \\ b_{ij} &= \begin{cases} |\omega_i| & \text{if } i = j, \\ 0 & \text{else,} \end{cases} \\ d_i &= \begin{cases} |\tau^n| |\omega_i| f_i^{n+1} & \text{if } \mathbf{x}_i \in \Omega \\ |\tau^n| \left(|\omega_i| f_i^{n+1} + \sum_{o \in \mathcal{B}(i)} |\gamma_o| \alpha g_i^{n+1} \right) & \text{if } \mathbf{x}_i \in \Gamma_N, \\ u_D(\mathbf{x}_i, t^n) & \text{if } \mathbf{x}_i \in \Gamma_D, \\ 0 & \text{else.} \end{cases} \end{aligned}$$

Remark 3.3. In practical applications one should keep in mind the following:

- (i) For the right-hand side f as well as for the inhomogeneous Neumann boundary condition g there was used only the midpoint rule to approximate the integrals. Since these functions are known one could use a higher order method, for instance, Gaussian quadrature.

- (ii) The convective term was discretized with a simple upwind scheme. For reasons of stability and accuracy, a higher order scheme should be used also here. In scope of the work an exponentially fitted upwind scheme will be implemented.
- (iii) The Dirichlet boundary condition was implemented only algebraically by means of setting the corresponding entries of the right-hand side equal to the Dirichlet condition and the ones of the in the diagonal of the stiffness matrix equal to 1.
- (iv) For the discretization a fully implicit time scheme was chosen. To achieve a higher order one could use, for example, a Crank-Nicholson scheme.
- (v) The resulting linear system is strictly diagonally dominant and, hence, there exists a uniquely defined solution.

3.4 The exponentially fitted upwind scheme

The convection from one discretization node to another across the boundary can be viewed as a one-dimensional problem. Since in finite volume methods finite differences are eventually used to approximate derivatives, we formulate the problem as a finite difference. So we consider a stationary two-point boundary value problem without the reaction term and with homogeneous right-hand side because these terms do not matter in the derivation of the scheme. We also want to assume that the convection velocity is positive $b > 0$, as one can decide for each vertex whether to use a forward finite difference or a backward finite difference. The problem and the simple upwind finite difference scheme read then

$$-\alpha u'' + bu = 0, \quad -\alpha D^+ D^- u_i + b D^- u_i = 0,$$

where $D^+ u := (u_{i+1} - u_i)/h$ and $D^- u := (u_i - u_{i-1})/h$ are the *forward* and *backward finite difference*, respectively. For simplicity, the mesh width h is chosen to be constant but is no constraint on the method.

The simple upwind scheme is known to be stable but it is only of first order convergence outside (boundary) layers. Inside layers, one can show that the scheme does not converge, see Roos et al. [26, chapter 2.1], where most of the identities of this section come from. Hence, we seek a uniform, and possibly higher, convergence rate in the whole domain. To this end, the scheme is reformulated:

$$-\left(\alpha + \frac{bh}{2}\right) D^+ D^- u_i + b D^0 u_i = 0,$$

where $D^0 u := (u_{i+1} - u_{i-1})/2h$ is the *central finite difference*. This is the central difference scheme applied to an equation with $-(\alpha + bh/2)$ being the diffusion coefficient. This means the simple upwind scheme can be understood as a central difference scheme applied to a modified problem; in the literature commonly referred to as a scheme with *artificial diffusion*. The idea is now to add the right amount of artificial diffusion to get the desired properties because if too much diffusion is added the layer gets smeared. A generalization is given by

$$-\alpha\sigma(q(x_i))D^+ D^- u_i + b_i D^0 u_i = 0$$

with the so-called *fitting factor* σ and $q(x) := bh/(2\alpha)$. The simple upwind scheme can be recovered by setting $\sigma(q) = 1 + q$. A careful investigation of the analysis of the convection-dominated equation and of the numerical analysis of the schemes considered so far lead to the choice (see Roos et al. [26, chapter 2.1] for details)

$$\sigma(q(x)) = q(x) \coth(q(x)).$$

Note that there holds $\lim_{q \rightarrow \infty} \coth(q) = 1$ and $\lim_{q \rightarrow -\infty} \coth(q) = -1$. As a consequence, for $\alpha \rightarrow 0$ this scheme turns into the simple upwind scheme.

Starting with the regular formulation of the simple upwind scheme but by already adding a fitting factor σ^* for the diffusion term, one can derive the condition to be

$$\sigma^*(q) = B(2q(x)),$$

with the *Bernoulli function* $B(z) := z/(e^z - 1)$. This is also the formulation used in finite volume methods, see Fuhrmann and Langmach [6]. Also common for finite volume methods is treating the convection and diffusion terms together. Introducing the function

$$\zeta(a) := \frac{1}{2}|a| - \frac{1}{2}a + 1 = \begin{cases} 1 - a, & a \leq 0, \\ 1, & a > 0, \end{cases}$$

and setting $a := (\mathbf{b} \cdot \mathbf{h}_{ij})/\alpha$, we can make the approximation

$$\int_{\gamma_{ij}} (-\alpha \nabla u + \mathbf{b}u) \cdot \mathbf{n}_{ij} \, dS(x) \approx \sum_{j \in \mathbf{nb}(i)} \alpha \frac{|\gamma_{ij}|}{h_{ij}} \left(\zeta \left(-\frac{\mathbf{b} \cdot \mathbf{h}_{ij}}{\alpha} \right) u_i^{n+1} - \zeta \left(\frac{\mathbf{b} \cdot \mathbf{h}_{ij}}{\alpha} \right) u_j^{n+1} \right).$$

By replacing $\zeta(a)$ by the Bernoulli function we obtain the *exponentially-fitted finite volume discretization* for a scalar convection-diffusion-reaction equation:

$$\begin{aligned} |\tau^n| |\omega_i| f_i^{n+1} + |\tau^n| \sum_{o \in \mathcal{B}(i)} |\gamma_o| \alpha g_i^{n+1} &= |\omega_i| (u^{n+1} - u^n) \\ &+ |\tau^n| \alpha \sum_{j \in \mathbf{nb}(i)} \frac{|\gamma_{ij}|}{h_{ij}} \left(B \left(-\frac{\mathbf{b} \cdot \mathbf{h}_{ij}}{\alpha} \right) u_i^{n+1} - B \left(\frac{\mathbf{b} \cdot \mathbf{h}_{ij}}{\alpha} \right) u_j^{n+1} \right) \\ &+ |\tau^n| \sum_{o \in \mathcal{B}(i)} |\gamma_o| (\mathbf{b} \cdot \mathbf{n}_o) u_i^{n+1} + |\tau^n| |\omega_i| c u_i^{n+1}. \end{aligned}$$

3.5 The population balance equation

In this section we treat the population balance equation for the particle size distribution, Equation (2.43). The right-hand side is a functional and hence changes the type of the equation to a partial integro-differential equation as not only partial derivatives are involved, but the function is also integrated. This makes the mathematical analysis extremely difficult. Currently there is a lack of theorems available concerning the existence of analytical solutions for this equation. Consequently, numerical methods cannot be judged by numerical analysis but rather only validated by comparison with experimental data. The experimental setup will be discussed together with the numerical results. In the context of the finite volume method, the functional will be treated as a regular function. This is because for specific values of \mathbf{x} , ℓ , and t the functional will be evaluated and enters the discretized equation as a number. The method to evaluate the functional

will be presented briefly subsequently but it is quite expensive so that only the midpoint rule (and no higher order scheme) will be applied.

First, we recall the population balance equation for the number density, Equation (2.43),

$$\begin{aligned}
\partial_t f + u_r \partial_r f + u_z \partial_z f + \frac{X_\infty}{U_\infty \ell_\infty} G(c, T) \partial_\ell f \\
&= \frac{X_\infty}{U_\infty f_\infty} (A^+[f] + A^-[f]), & \mathbf{x} \in \Omega_{\text{cyl}}, t \in (0, t_{\text{end}}), \\
f(\mathbf{x}, \ell, t) &= \frac{6 \cdot 10^7}{f_\infty t_{\text{end}} V_r} f_{\text{seed}}(\ell), & \mathbf{x} \in \Gamma_{\text{in}}, t \in [0, t_{\text{end}}) \\
f(\mathbf{x}, \ell_{\text{min}}, t) &= \frac{B_{\text{nuc}}}{f_\infty G(c, T)}, & \mathbf{x} \in \Omega_{\text{cyl}}, t \in (0, t_{\text{end}}), \text{ if } G(c, T) > 0, \\
f(\mathbf{x}, \ell, 0) &= 0, & \mathbf{x} \in \Omega_{\text{cyl}}, \ell \in (\ell_{\text{min}}, \ell_{\text{max}}).
\end{aligned}$$

with Ω_{cyl} and Ω_ℓ as defined in Equation (2.42).

Analogous to the previous cases, we assume an admissible finite volume partition of Ω_{cyl} . Following the notation of the finite volume method, we define $\mathbf{x}_i = (r_i, z_i)$ and denote the finite volumes of Ω_{cyl} by ω_i . The time interval is partitioned in time steps τ^n . Similarly, Ω_ℓ is partitioned in lengths $\ell_{\text{min}} = \ell_0 < \ell_1 < \dots < \ell_r = \ell_{\text{max}}$. In a consistent treatment one would define also finite volumes for the internal space Ω_ℓ by $\lambda_m = (\ell_{m-1/2}, \ell_{m+1/2})$, $0 < m < r$, but this would lead to an unstable scheme. The following necessary correction would result in the same scheme we get directly by a finite difference approximation. In regard of the two-dimensional case, recalling that the fluid velocity is divergence-free, the convective part can be rewritten in the following way:

$$u_r \partial_r f + u_z \partial_z f = \mathbf{u} \cdot \nabla f = \text{div}(\mathbf{u}f).$$

If not stated otherwise, \mathbf{u} will denote from now on the velocity as used in this equation; same holds for all differential operators like ∇ and div . Note also that Ω_{cyl} is a tensor product of intervals and therefore can be treated like a Cartesian domain.

We start the discretization with the integration over some volume ω_i and some time interval τ^n :

$$\begin{aligned}
&\int_{\tau^n} \int_{\omega_i} \frac{X_\infty}{U_\infty f_\infty} (A^+[f] + A^-[f]) \, d\mathbf{x} \, dt \\
&= \int_{\tau^n} \int_{\omega_i} \left(\partial_t f + \text{div}(\mathbf{u}f) + \frac{X_\infty}{U_\infty \ell_\infty} G(c, T) \partial_\ell f \right) \, d\mathbf{x} \, dt \\
&= \int_{\omega_i} \int_{\tau^n} \partial_t f \, dt \, d\mathbf{x} + \int_{\tau^n} \int_{\omega_i} \text{div}(\mathbf{u}f) \, d\mathbf{x} \, dt \\
&\quad + \int_{\tau^n} \int_{\omega_i} \frac{X_\infty}{U_\infty \ell_\infty} G(c, T) \partial_\ell f \, d\mathbf{x} \, dt
\end{aligned}$$

Here we changed the order of integration by Fubini's rule and define analogue to the previous cases $f_{i,m}^n = f(\mathbf{x}_i, \ell_m, t^n)$. Applying the fundamental theorem of calculus in the

first term and Gaussian's divergence theorem in the second leads to

$$\begin{aligned} &= \int_{\omega_i} (f^{n+1} - f^n) d\mathbf{x} + \int_{\tau^n} \left(\sum_{j \in \mathbf{nb}(i)} \int_{\gamma_{ij}} f \mathbf{u} \cdot \mathbf{n}_{ij} dS(\mathbf{x}) \right) dt \\ &\quad + \int_{\tau^n} \int_{\omega_i} \frac{X_\infty}{U_\infty \ell_\infty} G(c, T) \partial_\ell f d\mathbf{x} dt. \end{aligned}$$

Much like before the first term is approximated by the midpoint rule:

$$\int_{\omega_i} (f^{n+1} - f^n) d\mathbf{x} \approx |\omega_i| (f_{i,m}^{n+1} - f_{i,m}^n). \quad (3.15)$$

In the second term we apply the simple upwind scheme for the convective part and employ an implicit time scheme for the m -th internal coordinate:

$$\begin{aligned} &\int_{\tau^n} \left(\sum_{j \in \mathbf{nb}(i)} \int_{\gamma_{ij}} f \mathbf{u} \cdot \mathbf{n}_{ij} dS(\mathbf{x}) \right) dt \\ &\approx \int_{\tau^n} \left(\sum_{j \in \mathbf{nb}(i)} \frac{|\gamma_{ij}|}{h_{ij}} \xi(\mathbf{u}_{\gamma_{ij}} \cdot \mathbf{h}_{ij}) f_j - \xi(-\mathbf{u}_{\gamma_{ij}} \cdot \mathbf{h}_{ij}) f_i \right) dt \\ &\approx |\tau^n| \left(\sum_{j \in \mathbf{nb}(i)} \frac{|\gamma_{ij}|}{h_{ij}} \xi(\mathbf{u}_{\gamma_{ij}} \cdot \mathbf{h}_{ij}) f_{j,m}^{n+1} - \xi(-\mathbf{u}_{\gamma_{ij}} \cdot \mathbf{h}_{ij}) f_{i,m}^{n+1} \right). \end{aligned} \quad (3.16)$$

In the third term we use a simple upwind scheme, where we want to exploit the special structure of the growth rate, which plays an analogous role that the fluid velocity plays in the convective part. The growth rate is non-negative, i.e., either it is positive and we use the smaller neighbor or it is zero and does not contribute at all. In the finite volume context one would have used the fundamental theorem of calculus which would incorporate f at the midpoints $\ell_{m-1/2}$ and $\ell_{m+1/2}$ which, in turn, is not part of the approximating vector $(f_{i,m}^n)_{i,m,n}$. Hence, one would approximate these values by the neighboring values and obtain a central difference scheme. This scheme is known to be unstable, see the discussion of the simple upwind scheme on page 36. Therefore, we approximate the derivative by a simple upwind scheme directly:

$$\begin{aligned} &\int_{\tau^n} \int_{\omega_i} \frac{X_\infty}{U_\infty \ell_\infty} G(c, T) \left(f_{,m+\frac{1}{2}} - f_{,m-\frac{1}{2}} \right) d\mathbf{x} dt \\ &\approx \int_{\tau^n} \int_{\omega_i} \frac{X_\infty}{U_\infty \ell_\infty} G(c, T) \frac{f_{,m} - f_{,m-1}}{\ell_m - \ell_{m-1}} d\mathbf{x} dt \\ &\approx |\tau^n| |\omega_i| \lambda \frac{X_\infty}{U_\infty \ell_\infty} G(c_i^{n+1}, T_i^{n+1}) \frac{f_{i,m}^{n+1} - f_{i,m-1}^{n+1}}{\ell_m - \ell_{m-1}}. \end{aligned}$$

The right-hand side is approximated by a mid point rule for both the integral over ω_i and λ_m ; as in all other terms of the equation an implicit time scheme is employed:

$$\int_{\tau^n} \int_{\lambda_m} \int_{\omega_i} \frac{X_\infty}{U_\infty f_\infty} (A^+[f] + A^-[f]) d\mathbf{x} d\ell dt \approx |\tau^n| |\lambda_m| |\omega_i| \frac{X_\infty}{U_\infty f_\infty} (A^+[f_{i,m}^{n+1}] + A^-[f_{i,m}^{n+1}]).$$

Collecting all four approximations, we obtain the finite volume discretization of the population balance equation:

$$\begin{aligned}
& |\omega_i| |\lambda_m| (f_{i,m}^{n+1} - f_{i,m}^n) + |\tau^n| |\omega_i| \frac{X_\infty}{U_\infty \ell_\infty} G(c_i^{n+1}, T_i^{n+1}) \frac{f_{i,m}^{n+1} - f_{i,m-1}^{n+1}}{\ell_m - \ell_{m-1}} \\
& + |\tau^n| |\lambda_m| \left(\sum_{j \in \text{nb}(i)} \frac{|\gamma_{ij}|}{h_{ij}} \xi(\mathbf{u}_{\gamma_{ij}} \cdot \mathbf{h}_{ij}) f_{j,m}^{n+1} - \xi(-\mathbf{u}_{\gamma_{ij}} \cdot \mathbf{h}_{ij}) f_{i,m}^{n+1} \right) \\
& = |\lambda_m| |\omega_i| |\tau^n| \frac{X_\infty}{U_\infty f_\infty} (A^+[f_{i,m}^{n+1}] + A^-[f_{i,m}^{n+1}]).
\end{aligned} \tag{3.17}$$

Note that as there is no Neumann boundary this is not treated here. Much like in the case of convection-diffusion-reaction equations the Dirichlet boundary condition is incorporated algebraically.

3.6 Evaluation of the Aggregation Functional

The right-hand side of the population balance equation is a functional, meaning integrals have to be evaluated for every time step and spatial grid-point. In view of the computational cost, it is essential to have a fast algorithm for this task. The right-hand side of the population balance equation is given by (see Equations (2.43), (2.16), (2.14), (2.15), and (2.11))

$$A^+(V)[f_V] + A^-(V)[f_V]$$

with

$$\begin{aligned}
A^+(V)[f_V] &= \int_0^V K(V - V', V') f_V(V - V') f_V(V') dV', \\
A^-(V)[f_V] &= -f_V(V) \int_0^{V_{\max}} K(V, V') f_V(V') dV',
\end{aligned}$$

and

$$K(V, V') = \left(\sqrt[3]{V} + \sqrt[3]{V'} \right) \left(\frac{1}{\sqrt[3]{V}} + \frac{1}{\sqrt[3]{V'}} \right) + \sqrt{2 \nabla \mathbf{u} : \nabla \mathbf{u}} \left(\sqrt[3]{V} + \sqrt[3]{V'} \right).$$

For convenience, all constants and factors are replaced by 1 and the explicit dependency on \mathbf{x} and t is omitted because none of that is significant for the basic understanding of the algorithm described here. The function f will be approximated by a piecewise constant ansatz function with, say, n being the degrees of freedom. Usually one would divide each integral in $\mathcal{O}(n)$ subintervals where $f_V(V - V') f_V(V')$ is constant. This approach leads to at least $\mathcal{O}(n^2)$ arithmetical operations, where this has to be performed for every time step and every spatial grid point. This results either in a too expensive or inaccurate method. The method described briefly here represents a considerable improvement. It is taken from the works of Hackbusch [8] and [9] where it is explained in detail and further references can be found. Compared with the evaluation of $A^+(V)[f_V]$, the cost of evaluating $A^-(V)[f_V]$ is rather small and the same method used for the birth term A^+ can be applied to the sink term A^- . Hence, it will not be treated here.

Two features are essential for the algorithm: First, the aggregation kernel is separable and second, the grid is chosen to be locally equidistant. By saying the aggregation kernel is **separable**, we mean that there is a natural number k (the separation rank) such that the kernel can be written in the following form:

$$K(V, V') = \sum_{i=1}^k \alpha_i(V) \beta_i(V').$$

For instance, the Brownian aggregation kernel (first summand) is separable with separation rank 3: $\alpha_1 = \beta_1 = \sqrt{2}$, $\alpha_2 = 1/\sqrt[3]{V}$, $\beta_2 = \sqrt[3]{V'}$, $\alpha_3 = \sqrt[3]{V}$, $\beta_3 = 1/\sqrt[3]{V'}$. Thus, the birth rate caused by aggregation can be expressed as

$$A^+(V)[f_V] = \int_0^V \left(\sum_{i=1}^k \alpha_i(V - V') \beta_i(V') \right) f_V(V - V') f_V(V') dV'.$$

Now we combine $\alpha_i(V - V')$ and $f_V(V - V')$ on one hand and $\beta_i(V')$ and $f_V(V')$ on the other hand; denoted by $\varphi_i(V - V')$ and $\psi_i(V')$ respectively. Then the integral can be restated as a sum of convolutions:

$$\begin{aligned} A^+(V)[f_V] &= \int_0^V \left(\sum_{i=1}^k \varphi_i(V - V') \psi_i(V') \right) dV' = \sum_{i=1}^k \int_0^V \varphi_i(V - V') \psi_i(V') dV' \\ &= \sum_{i=1}^k \underbrace{(\varphi_i * \psi_i)(V)}_{=: \omega_i(V)}. \end{aligned}$$

For now we consider only one summand $\omega(V) = (\varphi * \psi)(V)$ and an equidistant grid: $V_j = jh$, $1 \leq j \leq n$, $h = \frac{1}{n}$. Piecewise constant functions are used to approximate φ and ψ (or a projection there of), such that they are given by their values φ_j, ψ_j on the intervals (V_{j-1}, V_j) ($1 \leq j \leq n$). Hence, ω is a piecewise linear function and completely known if it is evaluated at all points V_j . This leads to the representation of $\omega(V_j)$ as a sum:

$$\omega(V_j) = h \sum_{m=1}^j \varphi_m \psi_{j-m+1}, \quad (1 \leq j \leq n).$$

In essence, for solving this problem three fast Fourier transforms are necessary. These can be performed with complexity $\mathcal{O}(n \log n)$. Since this has to be done for all k sums this leads to $\mathcal{O}(kn \log n)$.

In the pipe there are much more small particles contained than large particles such that the fine scales are not needed for larger particles. This leads to the idea of refining the grid towards zero and the second important feature. With *locally equidistant* we mean that the grid may be decomposed in several grids where each grid is equidistant. An illustration of such a grid is given in Figure 3.1.

On each level of the hierarchical grid a basis consisting of piecewise constant and pairwise orthogonal functions was chosen (orthogonality with respect to the L^2 inner product). The idea is now to apply the method described above on each of the levels. The complexity is

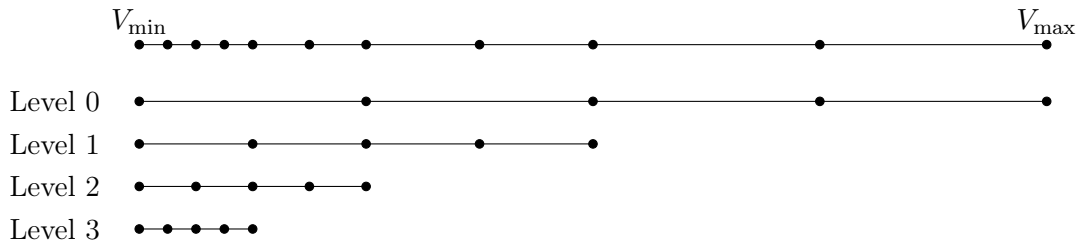


Figure 3.1: Illustration of the graded grid.

roughly the same, but more grid points towards zero can be chosen and attain a better accuracy. See Hackbusch [8] and [9] for an extension to higher order polynomials and implementation details. Also important to note is that the method is implemented in a way that ensures mass conservation which is the main concern of the latter referenced work.

4 Numerical Experiments

In this section we want to test the method described above. First, there are some simple examples to assure that the program works properly. After that there are some experiments with cases which are commonly used to analyze certain properties of algorithms in the context of convection-dominated convection-diffusion problems.

Most examples are defined on $\Omega = (0, 1)^2$ with boundary $\Gamma := \partial\Omega$. For convenience, each part of the boundary is assigned as follows:

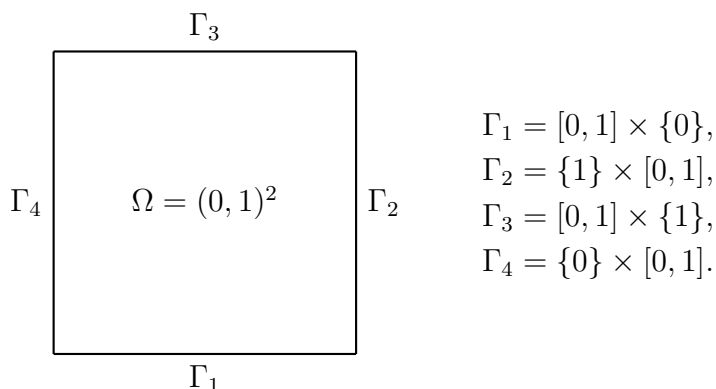


Figure 4.1: Illustration of the computational domain for the test cases.

The grid was chosen to consist of uniform quadrangles as illustrated below. It starts with a unit square with four nodes at the corners as can be seen in Figure 4.1. One uniform refinement leads to four squares with nine nodes, another refinement to 16 squares and 25 nodes, see Figures 4.2 and 4.3. For each node a finite volume is constructed: Determine the orthogonal lines to the discretization edges and then the intersections of the perpendiculars. These intersections, also referred to as *grid corners*, are the corners of the finite volumes. The orthogonality can be observed in Figures 4.2 and 4.3.

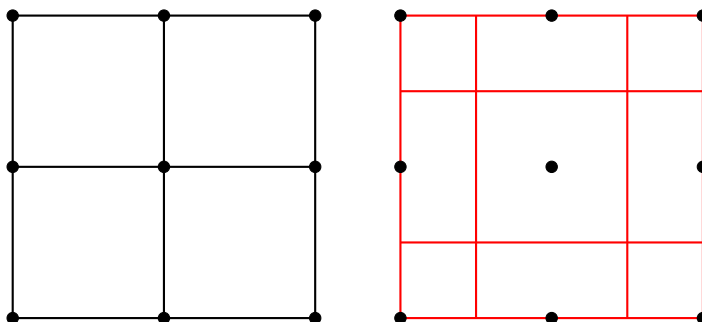


Figure 4.2: Illustration of the finite volume grid after one refinements. Left: vertices with discretization edges; right: vertices with finite volumes.

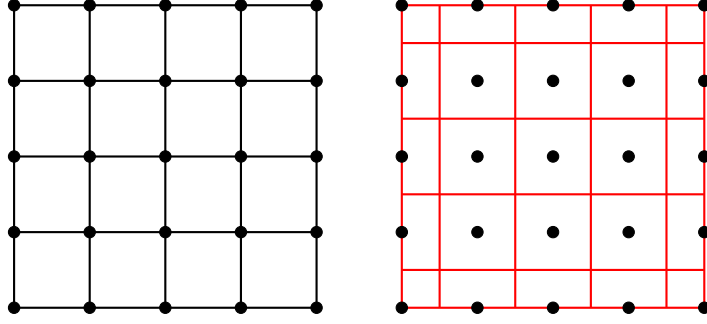


Figure 4.3: Illustration of the finite volume grid after two refinements. Left: vertices with discretization edges; right: vertices with finite volumes.

4.1 Linear Solution

The first example is defined as follows:

$$\left. \begin{aligned}
 \partial_t u - \alpha \Delta u &= 0 && \text{in } \Omega \times [0, T], \\
 u &= 0 && \text{on } \Gamma_1 \times [0, T], \\
 \nabla u \cdot n &= 0 && \text{on } \Gamma_2 \times [0, T], \\
 u &= 1 && \text{on } \Gamma_3 \times [0, T], \\
 u &= y && \text{on } \Gamma_4 \times [0, T], \\
 u(\cdot, 0) &= 0 && \text{in } \Omega,
 \end{aligned} \right\} \text{Example 4.1}$$

with exact solution $u(x, y) = y$. This case is chosen because its analytical solution can be represented exactly by a combination of linear functions, such that the obtained solution should converge to the exact solution up to machine precision. Although the solution is stationary, the instationary equation was chosen, in order to observe convergence with respect to time. The parameters are $\alpha = 0.01$, $\Delta t = 0.1$ s, $N = 128$, and the error tolerance was set to 10^{-14} .

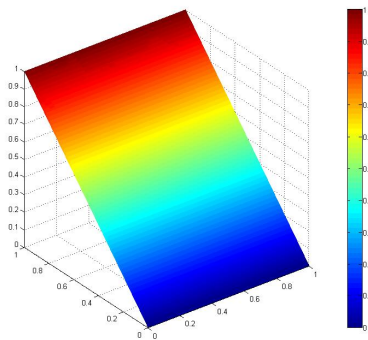


Figure 4.4: Computed solution of Example 4.1 after 322 s simulation time with error tolerance 10^{-14} .

As one might expect, the solution in Figure 4.4 looks just like the exact solution $u(x, y) = y$ and for this setting of the coefficients and parameters the error tolerance of 10^{-14} was reached after 322 s, even though it started to oscillate after 290 s with an error of $1.3 \cdot 10^{-14}$.

Since this example works fine we can go on to more complex problems.

4.2 Quadratic Solution

This problem serves to analyze the convergence rate of the method with respect to the mesh width and to compare the simple upwind scheme with the exponentially fitted upwind scheme. The problem is defined as follows:

$$\left. \begin{aligned} -\alpha\Delta u + \mathbf{b} \cdot \nabla u + cu &= f && \text{in } \Omega \times [0, T], \\ u &= x^2 && \text{on } \Gamma_1 \times [0, T], \\ u &= y^2 + 1 && \text{on } \Gamma_2 \times [0, T], \\ u &= x^2 + 1 && \text{on } \Gamma_3 \times [0, T], \\ u &= y^2 && \text{on } \Gamma_4 \times [0, T], \\ u(\cdot, 0) &= 0 && \text{in } \Omega . \end{aligned} \right\} \text{Example 4.2}$$

The problem is constructed so that the solution is given by

$$u(x, y) = x^2 + y^2$$

resulting in

$$f(x, y) = -4\alpha + 2b_x x + 2b_y y + c(x^2 + y^2).$$

The solution is shown in Figure 4.5. We also want to investigate the influence of the

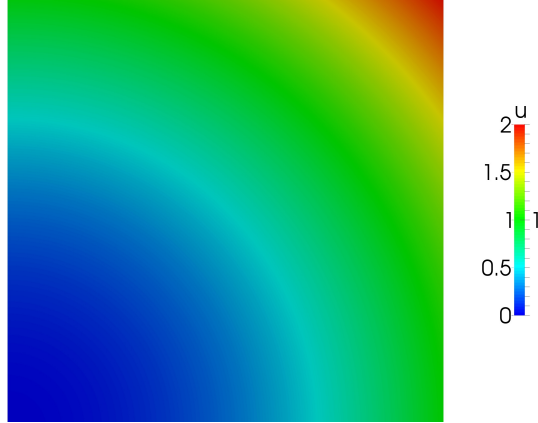


Figure 4.5: Solution to Example 4.2

diffusion constant α , the convection, and the reaction. Figure 4.6 shows the L^2 -error of the pure diffusive case, i.e., $\mathbf{b} = (0, 0)^T$ and $c = 0$, and the corresponding L^2 -errors of convection-diffusion-reaction cases with $\alpha \in \{10^{-3}, 10^{-6}\}$, $\mathbf{b} = (1, 1)^T$, $c = 1$, solved with both the simple and the exponentially fitted upwind scheme.

It can be easily observed that the pure diffusive case has a constant convergence rate and outperforms the other cases. Determined by this log-log plot, the convergence rate for the pure diffusive case is 2. That means when the mesh width is halved, the error decreases

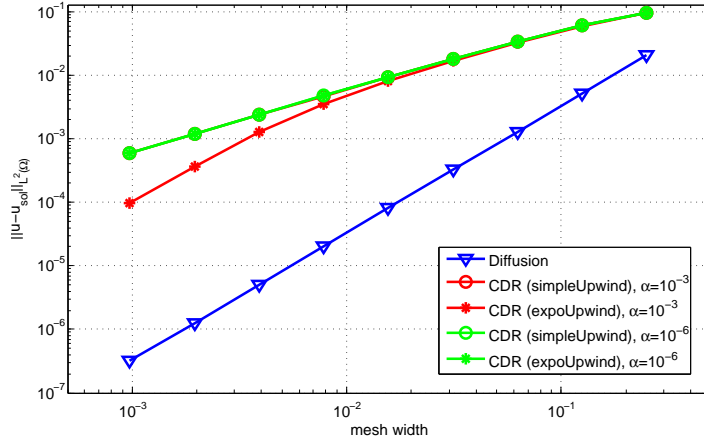


Figure 4.6: The convection-diffusion-reaction case in comparison with the pure diffusion case.

by a factor of 4. This is the same result one would obtain with classic finite elements or finite differences. Next, all other cases seem to have the same behavior in the beginning, but in the end the error for the case with $\alpha = 10^{-3}$ solved by the exponentially fitted upwind scheme decreases more rapidly. There the convergence rate is between the first two grids approximately 0.69 and between the last two grids 1.93. The remaining three cases seem to have the same values. In fact, figure 4.7 shows a close up of them: Their values differ only little. The convergence rate in all these three cases is between the first two grids approximately 0.68 and between the last two grids 1.

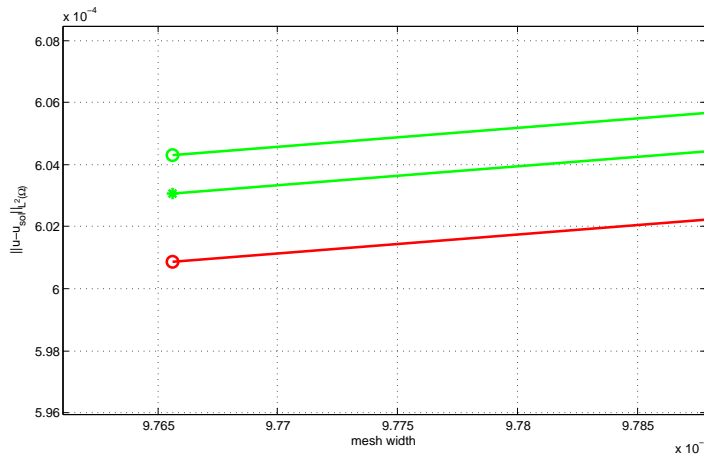


Figure 4.7: L^2 -error for the convection-diffusion-reaction cases with (i) $\alpha = 10^{-6}$, simple upwind scheme; (ii) $\alpha = 10^{-6}$, exponentially fitted upwind scheme; (iii) $\alpha = 10^{-3}$, simple upwind scheme (from top to bottom).

That means that the exponentially fitted upwind scheme has a better performance only if the diffusive constant is not too small compared to convection and/or reaction. Cases without reaction term have been also considered and they turn out to have the same behavior. Figure 4.8 shows all cases for this problem that have been solved with the exponentially fitted upwind scheme. Interestingly, the reaction term appears to 'simplify'

the problem since the corresponding errors are somewhat smaller than the ones of the convection-diffusion case.

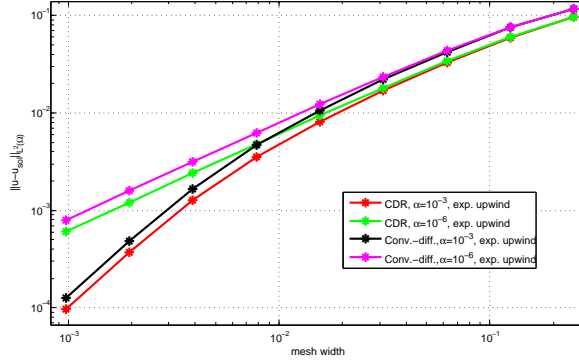


Figure 4.8: L^2 -error of all cases solved with the exponentially fitted upwind scheme. Impact of the diffusion constant on the convergence rate.

4.3 Heat equation with multiple Fourier series

This example is concerned with the solution of the heat equation by means of multiple Fourier series. It is based on an exercise stated by Coleman [5] and reads as follows:

$$\left. \begin{aligned} \partial_t u - \alpha \Delta u &= 13\pi^2 \alpha \sin(2\pi x) \sin(3\pi y) && \text{in } \Omega \times (0, T) \\ u &= 0 && \text{on } \Gamma \times [0, T] \\ u(x, y, 0) &= \sin(4\pi x) \sin(7\pi y) && \text{in } \Omega \end{aligned} \right\} \text{Example 4.3}$$

Using separation of variables, we make the following ansatz

$$u(x, y, t) = \sum_{n,m=1}^{\infty} T_{n,m}(t) \sin(n\pi x) \sin(m\pi y).$$

Inserting into the heat equation, making use of $\{\sin(n\pi x) \sin(m\pi y) | n, m \in \mathbb{N}\}$ being an orthonormal basis of $\{f \in L((0, 1)^2) | f|_{\partial\Omega} = 0\}$, and inserting the initial condition leads to the analytic solution:

$$u(x, y, t) = \sum_{n,m=1}^{\infty} (1 - e^{-13\alpha\pi^2 t}) \sin(2\pi x) \sin(3\pi y) + e^{-65\alpha\pi^2 t} \sin(4\pi x) \sin(7\pi y).$$

The second summand accounts for the initial condition. Note that the absolute value of the exponent of the second summand is larger than the one of the first one. Thus one can observe to some extent that at first the initial condition subsides and then the stationary solution develops. (If the constants were switched then the stationary solution would develop more rapidly than the initial condition would subside.) Since both terms with negative exponents tend to 0 as time evolves, the stationary solution is given by

$$u_{\text{stat}} = \sin(2\pi x) \sin(3\pi y).$$

In figure 4.8 the evolution of the L^2 -error of all grids with time step size $\tau = 0.1$ is represented. One can see the convergence on every level. Also in the beginning on finer grids the error increases and then decreases eventually. A solution is considered to be

Table 3: Time τ^* when the relative change of the solution from one time step to the next one is less than 10^{-6} depending on the mesh width h ; the final error compared with the exact solution; $\tau = 0.1$.

h	τ^*	$\ u(\tau^*) - u_{\text{sol}}(\tau^*)\ _{L^2(\Omega)}$
1/8	90.4	$3.6678 \cdot 10^{-2}$
1/16	97.7	$8.96501 \cdot 10^{-3}$
1/32	97.5	$2.22873 \cdot 10^{-3}$
1/64	105.1	$5.56395 \cdot 10^{-4}$
1/128	104.3	$1.39103 \cdot 10^{-4}$
1/256	122.9	$3.47621 \cdot 10^{-5}$

stationary when the relative change of the error from one time step to the next one is smaller than 10^{-6} . Table 3 shows when these values were reached and which values were attained.

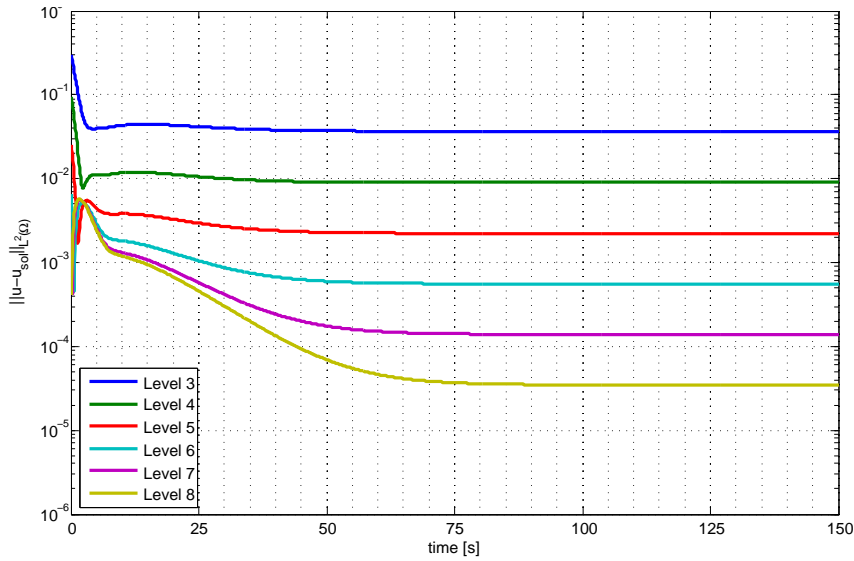


Figure 4.9: L^2 -error on all grids with time step size $\tau = 0.1$ s.

Further, figure 4.10 shows the impact of the time step size. Even though neither it effects stability nor the final error, it does alter the point of time *when* the solution becomes stationary and the error beforehand. This is also shown in table 4.

As one can see, a smaller time step size increases the accuracy before the final approximation on the corresponding grid is reached. Finally, figure 4.11 shows the convergence exemplarily for the time step size $\tau = 0.1$. As in the pure diffusive case considered in previous example the convergence rate is 2.

Table 4: Time τ^* when the relative change of the solution from one time step to the next one is less than 10^{-6} depending on the time step size τ ; the final error compared with the exact solution; dof = 66049.

τ	τ^*	$\ u(\tau^*) - u_{\text{sol}}(\tau^*)\ _{L^2(\Omega)}$
0.4	147.6	$3.47563 \cdot 10^{-5}$
0.2	135	$3.47582 \cdot 10^{-5}$
0.1	122.9	$3.47621 \cdot 10^{-5}$
0.05	110.75	$3.47706 \cdot 10^{-5}$

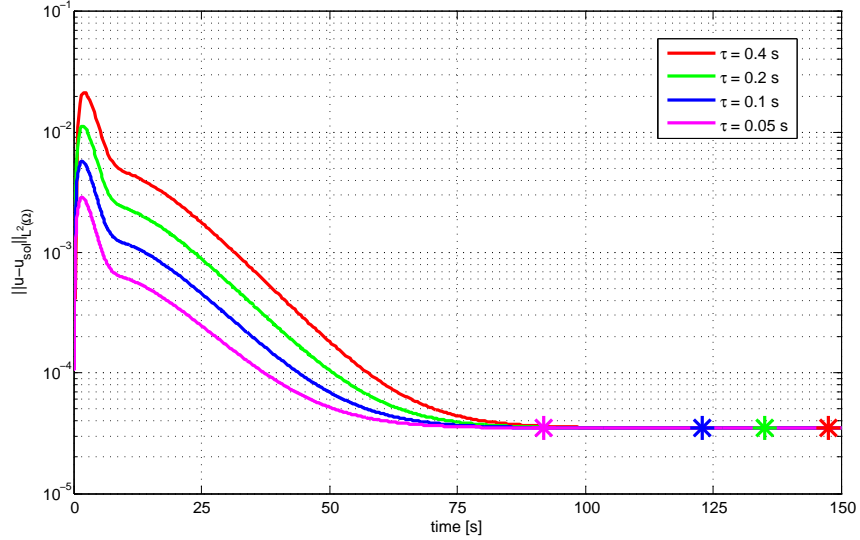


Figure 4.10: Evolution of the error for different choices of the time step size τ ; dof = 66049.

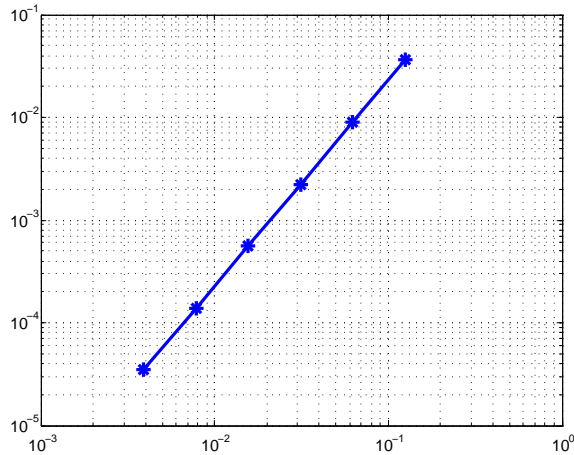


Figure 4.11: Convergence rate with respect to the mesh width; $\tau = 0.1$.

4.4 Sharp layers

In this example we want to investigate the behavior of the method in the presence of sharp layers. They occur because the diffusion coefficient (respectively the kinematic viscosity

or thermal diffusivity) is usually much smaller than the convection velocity. This example was proposed by Hughes et al. [12] and, for instance, also used by John et al. [18]. The problem reads as follows:

$$\begin{aligned} -\alpha\Delta u + \mathbf{b} \cdot \nabla u &= 0 && \text{in } \Omega \\ u &= 0 && \text{on } \Gamma \end{aligned}$$

with $\mathbf{b} = (\cos(-\pi/3), \sin(-\pi/3))$ and $\alpha \in \{10^{-3}, 10^{-6}\}$. The solution features an interior as well as a (exponential) boundary layer due to the choice of the boundary conditions and the convection velocity. Figures 4.12 and 4.13 show the solutions on level 5 and 10, respectively. In the 2D-color plot it is easy to observe the thickness of the interior layer whereas the boundary layer looks not properly represented in the first case and simply not visible in the latter. In a close up, as represented in figure 4.14, one can see that the complete transition from 0 to 1 takes place within one cell column.

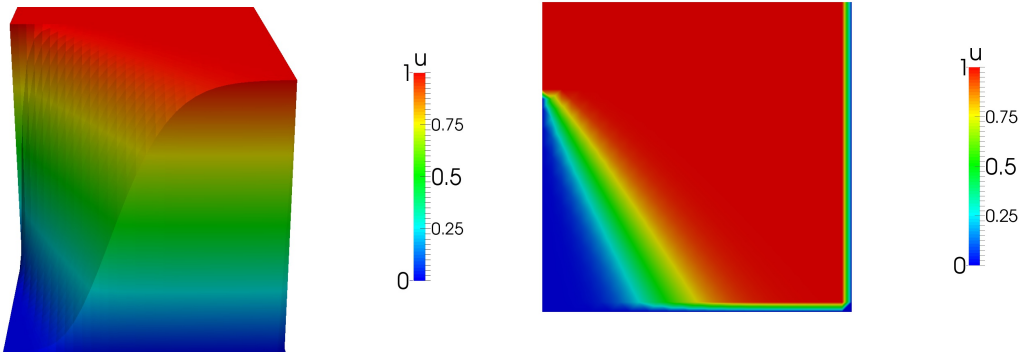


Figure 4.12: Solution to Example 3.4: $\alpha = 10^{-4}$, dof = 1089

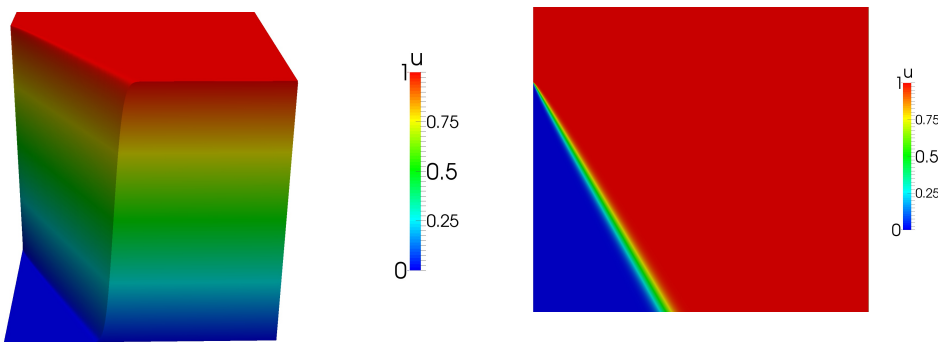


Figure 4.13: Solution to Example 3.4: $\alpha = 10^{-4}$, dof = 1050625

Since no analytical solution for that problem is known, only a qualitative analysis is possible. Nonetheless, it shows important features of the method. The most important qualities that all solutions share are:

- There are no over- or undershoots: There holds $0 \leq u(x, y) \leq 1 \quad \forall (x, y) \in \Omega$.
- There are no spurious oscillations.

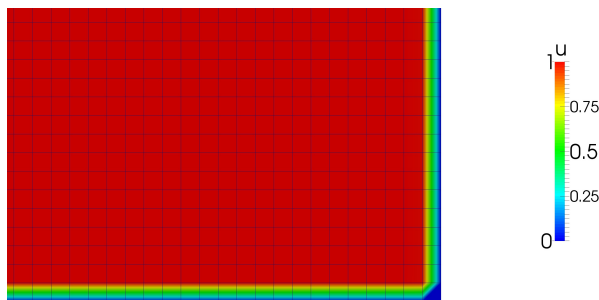


Figure 4.14: Close up of solution to Example 3.4: $\alpha = 10^{-4}$, dof = 1050625.

- The thickness of the boundary layer is exactly one cell width

The second point is a major drawback of finite element methods in the context of convection-dominated convection-diffusion equations as they lead to unphysical values like negative concentrations. The work of John et al. [18] is concerned with this issue and how it may be overcome, see there for further references.

Next we want to compare the simple upwind scheme with the exponentially fitted upwind scheme. Since they show the same behavior at the boundary layer we will focus on the interior layer. Figure 4.15 shows the solutions obtained with both methods. They seem

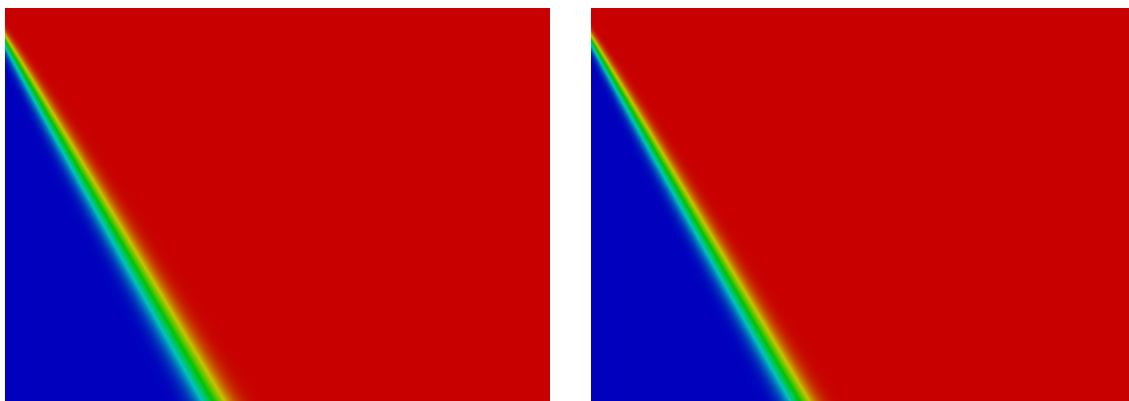


Figure 4.15: Interior layer of solution to Example 3.4: $\alpha = 10^{-4}$, dof = 1050625, solved with the simple upwind scheme (above) and the exponentially fitted upwind scheme (below).

to differ little and, in fact, they do, but if one zooms, one can see that the interior layer obtained with the exponentially fitted upwind scheme is somewhat thinner than the one obtained with the simple upwind scheme, see figure 4.16.

This problem was also analyzed with $\alpha = 10^{-6}$ and $\alpha = 10^{-3}$. Briefly, in the latter case the difference in thickness was more visible; in the first one no difference could be observed. Indeed, it appears that the solution obtained with the exponentially fitted upwind scheme for both $\alpha = 10^{-4}$ and $\alpha = 10^{-6}$ is the same and that the solution of the simple upwind scheme 'converges' towards the other solution with decreasing α .

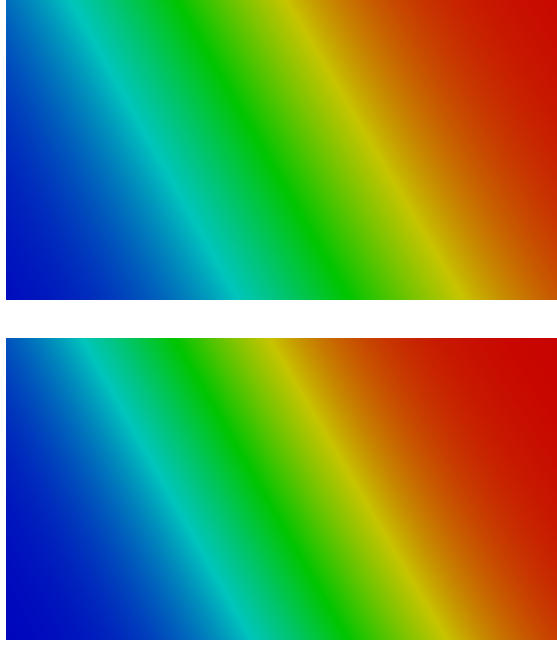


Figure 4.16: Interior layer of solutions to Example 3.4: $\alpha = 10^{-4}$, dof = 1050625, solved with the simple upwind scheme (above) and the exponentially fitted upwind scheme (below).

4.5 Numerical Solution of the Population Balance System

This section is concerned with the solution of the population balance system, but first the experiment will be presented briefly and the entity used to validate the algorithm discussed. Furthermore, it contains the solution of the conservation equations for the temperature and the concentration.

The experiment was conducted by Borchert and Sundmacher [4] with the aim of investigating aggregation with the help of image analysis. Urea crystals suspended in saturated ethanol solution flowing through a tube was the center of attention. The main components of the experiment are illustrated in Figure 4.17 and consisted of a vessel with crystal slurry (1), a seed crystal intake (2), an aggregation tube (3), and a flow cell microscope with imaging sensor (4). The experiment was basically pursued as follows: The vessel was filled with a crystal suspension and clear solution was pumped out of the vessel through the tube and the microscope's flow cell back into the vessel. Eventually seed crystals were injected into the solution, see Borchert and Sundmacher [4] for more details.

The experiments provide space-time-averaged data at the inlet, which was incorporated in the inlet condition, see Equation (2.29), and at the outlet, which was used to validate the method presented in this thesis. More precisely, the *space-time-averaged volume fraction* was determined, defined as

$$q_3(r, z, \ell, t) = \frac{\ell^3 f(r, z, \ell, t)}{\int_{\ell_{\min}}^{\ell_{\max}} \ell^3(r, z, \ell, t) d\ell}.$$

In the algorithm, a steady state solution after 1000 s could be observed such that the solution at this time was used as a basis to compute the volume fraction. Since in the

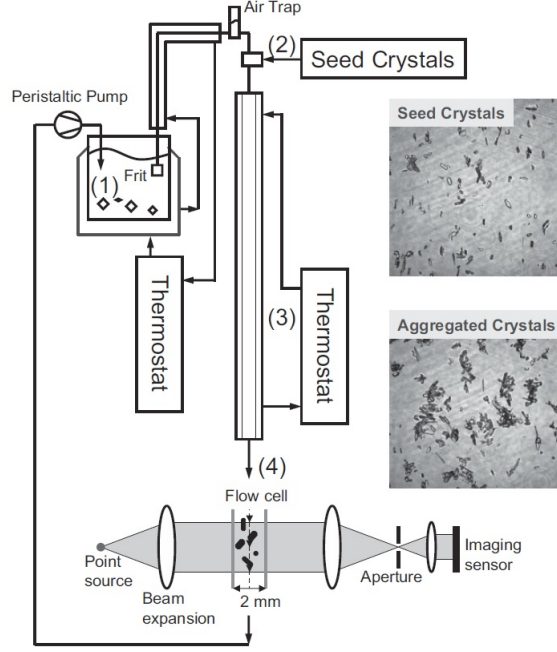


Figure 4.17: The experimental setup (Borchert and Sundmacher [4]).

experiments the data at the outlet was used to determine q_3 , this was also done in the computations, namely at $z = 200$. For every particle diameter ℓ_m , the numerical solution $f(r, 200, \ell_m, 1000)$ was then averaged with respect to r .

The population balance system is given by the population balance equation for the particle size distribution, Equation (2.43), accompanied by convection-diffusion-reaction equations for the temperature and concentration, Equations (2.44) and (2.45) respectively, and the Hagen-Poiseuille flow, Equation (2.41). They form a coupled system as the particle growth rate depends on the concentration and temperature and is involved in all three equations; the particle size distribution appears in the reaction term of both phase variables. The solution strategy follows the approach pursued by Hackbusch et al. [10] and Anker et al. [1] and will be presented briefly.

This system was solved with the research code MoonMD, created by John and Matthies [15] and developed at the Weierstrass Institute for Applied Analysis and Stochastics. For the conservation equations available methods were used. For the whole system an implicit time scheme was chosen, so consider the time t^{n+1} . First, the population balance equation was decoupled from the two conservation equations by using the particle size distribution from the previous time f^n . The temperature and the concentration, still coupled, were solved iteratively by first computing the temperature with c^n and f^n and then the concentration with c^{n+1} and f^n . Since these equations are convection-dominated appropriate methods have to be used. Therefore, the linear finite element flux-corrected transport (FEM-FCT) scheme was used, see Kuzmin [20]. John and Schmeier [16] and [17] show that this method belongs to the best performing ones for transient convection-dominated scalar equations. The population balance equation was solved with the finite volume method presented in this thesis using the current solutions for temperature T^{n+1} and concentration c^{n+1} .

For the discretization a structured grid was used, consisting of rectangles in the case of the conservation equations and cuboids in the case of the population balance equation. The spatial grid on the first level was made of 67×13 discretization points and was uniformly refined, see Table ?? for the number of degrees of freedom on different levels. The grid with respect to the internal grid was always made of 94 discretization points and chosen to be equidistant for the left-hand side. For the right-hand side the grid was transformed to meet certain properties required by the algorithm used to evaluate the aggregation functional, see chapter 3.6 and Hackbusch [8], [9].

In Figure 4.18 the space-time averaged volume fractions obtained by the experiment and by numerical simulation are shown. The immediate observation is, unfortunately, they do not coincide. More precisely, the curve based on the numerical solution is too steep in the beginning and, therefore, attains its maximum too early. Also, the right part of the curve does not match the experimental data; the slope is not steep enough such that the whole curve is too wide in general. Furthermore, since both curves are normed, one cannot see if they have the same order of magnitude. Also in this regard the result is not satisfying as the difference is of three orders of magnitude. This means, quantitatively, that in the numerical simulation far too many particles appear and, qualitatively, especially the ratio of the very small particles to the number overall is too large.

Although various possible causes were pursued, none led to resolving the error. The mesh size as well as the time step size (0,1 s and 1 s) did not influence the result significantly. At the end, the question for this behavior must be left open.

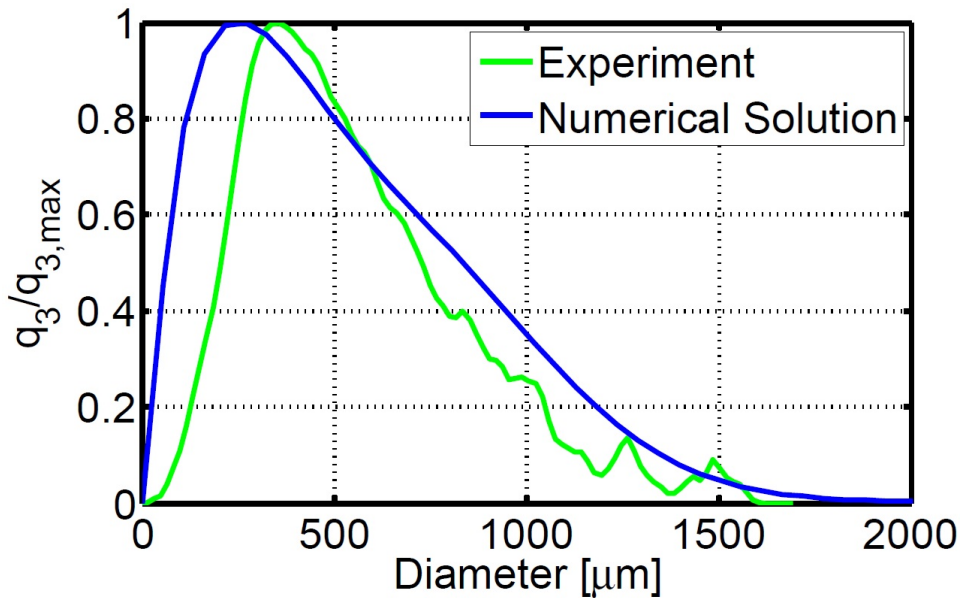


Figure 4.18: Normed space-time averaged volume fractions of the experiment and the numerical solution.

5 Conclusions and Outlook

In this thesis a population balance system (PBS) was considered. At first, it consisted of the Navier-Stokes equations, non-linear convection-diffusion-reaction equations for the temperature and the concentration, and a population balance equation (PBE) for the particle size distribution (PSD). These were derived and subsequently simplified by choosing appropriate coordinates, reducing the spatial dimension by one and resulting in an analytic solution for the fluid flow. The main goal of this work was the numerical solution of the PBE by means of a finite volume method. Since no analytic solution for this problem is known, experimental data was used to validate the algorithm. In the end, the approximation proved to be rather coarse and in need of improvement, although the results for convection-dominated convection-diffusion-reaction equations were good. In fact, an exponentially-fitted upwind scheme was employed and exemplarily it was shown that, if the diffusion coefficient is not too small, it leads to a higher convergence rate compared with the simple upwind scheme. For vanishing diffusion both schemes yield the same results.

Besides the improvement of the algorithm, there are other courses which can be taken in future research. First, the method can be extended to a three-dimensional spatial version which can be also used to verify whether the model error caused by the assumptions made in this thesis are negligible. Similarly, more internal coordinates can be of interest to obtain a more representative model for particulate flows. Also, in this work a laminar flow was considered which opens the question for turbulent flows. Research in this direction has already been done, for instance, by Schmeyer [29]. From a more applied point of view, the application in other fields like meteorology or biological cultures could be of interest. The finite volume method can also be extended to be applicable to complex geometries.

References

- [1] Felix Anker, Sashikumaar Ganesan, Volker John, and Ellen Schmeyer. “A comparative study of a direct discretization and an operator-splitting solver for population balance systems”. In: *Computers & Chemical Engineering* 75 (2015), pp. 95–104. DOI: <http://dx.doi.org/10.1016/j.compchemeng.2015.01.010>.
- [2] George K. Batchelor. *An Introduction to Fluid Dynamics*. Cambridge University Press, 1967.
- [3] R. Byron Bird, Warren E. Stewart, and Edwin N. Lightfoot. *Transport phenomena*. Second edition. New York: John Wiley & Sons, Inc., 2002. ISBN: 0-471-41077-2.
- [4] Christian Borchert and Kai Sundmacher. “Crystal Aggregation in a Flow Tube: Image-Based Observation”. In: *Chemical Engineering & Technology* 34.4 (2011), pp. 545–556. DOI: 10.1002/ceat.201000465.
- [5] Matthew P. Coleman. *An Introduction to Partial Differential Equations with MATLAB*. Second Edition. Chapman and Hall/CRC, 2013. ISBN: 978-1-4398-9847-5.
- [6] Jürgen Fuhrmann and Hartmut Langmach. “Stability and existence of solutions of time-implicit finite volume schemes for viscous nonlinear conservation laws”. In: *Applied Numerical Mathematics* 37.1-2 (2001), pp. 201–230. DOI: [http://dx.doi.org/10.1016/S0168-9274\(00\)00039-8](http://dx.doi.org/10.1016/S0168-9274(00)00039-8).
- [7] Morton E. Gurtin, Eliot Fried, and Lallit Anand. *The Mechanics and Thermodynamics of Continua*. Cambridge University Press, 2010.
- [8] Wolfgang Hackbusch. “On the Efficient Evaluation of Coalescence Integrals in Population Balance Models”. In: *Computing* 78.78 (2006), pp. 145–159. DOI: 10.1007/s00607-006-0174-2.
- [9] Wolfgang Hackbusch. “Approximation of Coalescence Integrals in Population Balance Models with local mass Conservation”. In: *Numerische Mathematik* 106.4 (2007), pp. 627–657. DOI: 10.1007/s00211-007-0077-y.
- [10] Wolfgang Hackbusch, Volker John, Aram Khachatryan, and Carina Suci. “A numerical method for the simulation of an aggregation-driven population balance system”. In: *International Journal for Numerical Methods in Fluids* 69.10 (2012), pp. 1646–1660. DOI: 10.1002/flid.2656.
- [11] Sam Howison. *Practical Applied Mathematics: Modelling, Analysis, Approximation*. Cambridge University Press, 2005.
- [12] Thomas J.R. Hughes, Michel Mallet, and Mizukami Akira. “A new finite element formulation for computational fluid dynamics: II. Beyond SUPG”. In: *Computer Methods in Applied Mechanics and Engineering* 54.3 (1986), pp. 341–355. DOI: [http://dx.doi.org/10.1016/0045-7825\(86\)90110-6](http://dx.doi.org/10.1016/0045-7825(86)90110-6).
- [13] Mikhail Itskov. *Tensor Algebra and Tensor Analysis for Engineers*. Springer, 2007. ISBN: 978-3-540-36046-9.
- [14] V John, I Angelov, AA Öncül, and Thévenin D. “Techniques for the reconstruction of a distribution from a finite number of its moments”. In: *Chemical Engineering Science* 62 (2007), pp. 2890–2904.
- [15] Volker John and Gunar Matthies. “MoonNMD – a program package based on mapped finite element methods”. In: *Computing and Visualization in Science* 6.2 (2004), pp. 163–170.

- [16] Volker John and Ellen Schmeyer. “Stabilized finite element methods for time-dependent convection?diffusion-reaction equations”. In: *Computer Methods in Applied Mechanics and Engineering* 198 (2008), 475?–494.
- [17] Volker John and Ellen Schmeyer. “On finite element methods for 3d time-dependent convection?diffusion-reaction equations with small diffusion”. In: *BAIL 2008 - Boundary and Interior Layers, Lecture Notes in Computational Science and Engineering* Vol. 69 (2009), pp. 173–182.
- [18] Volker John, Petr Knobloch, and Simona B. Savescu. “A posteriori optimization of parameters in stabilized methods for convection?diffusion problems ? Part I”. In: *Computer Methods in Applied Mechanics and Engineering* 200 (2011), pp. 2916 – 2929. DOI: <http://dx.doi.org/10.1016/j.cma.2011.04.016>.
- [19] Konrad Königsberger. *Analayis 2*. Fifth edition. Springer, 2004. ISBN: 3-540-20389-3.
- [20] Dmitri Kuzmin. “Explicit and implicit FEM-FCT algorithms with flux linearization”. In: *Journal of Computational Physics* 228.7 (2009), pp. 2517 –2534. DOI: <http://dx.doi.org/10.1016/j.jcp.2008.12.011>.
- [21] D Marchisio and R. Fox. “Solution of population balance equations using the direct quadrature method of moments”. In: *Journal of Aerosol Science* 36 (2005), pp. 43–73.
- [22] R. McGraw. “Description of aerosol dynamics by the quadrature method of moments”. In: *Aerosol Science and Technology* 27 (1997), pp. 255–265.
- [23] Wolfgang H. Müller. *Streifzüge durch die Kontinuumstheorie*. Springer, 2011. ISBN: 978-3-642-19869-4. DOI: 10.1007/978-3-642-19870-0.
- [24] Doraiswami Ramkrishna. *Population Balances*. Academic Press, 2000.
- [25] Alan D. Randolph and Maurice A. Larson. *Theory of Particulate Processes*. Second edition. Academic Press, Inc., 1988.
- [26] H.-G. Roos, M. Stynes, and L. Tobiska. *Numerical Methods for Singularly Perturbed Differential Equations: Convection-Diffusion and Flow Problems*. 1996. ISBN: 978-3-662-03208-4. DOI: 10.1007/978-3-662-03206-0.
- [27] Kendree J. Sampson and Doraiswami Ramkrishna. “Particle size correlations in brownian agglomeration. Closure hypotheses for product density equations”. In: *Journal of Colloid and Interface Science* 110.2 (1986), pp. 410–423.
- [28] Heinz Schade, Ewald Kunz, Frank Kameier, and Christian O. Paschereit. *Strömungslehre*. Fourth edition. De Gruyter, 2013. ISBN: 978-3110292213.
- [29] Ellen Schmeyer. *Numerische Verfahren zur Simulation von Mehrphasenströmungen mittels Populationsbilanzen*. PhD thesis, 2012.
- [30] Marian von Smoluchowski. “Versuch einer mathematischen Theorie der Koagulationskinetik kolloidaler Lösungen”. In: *Zeitschrift für physikalische Chemie* 92.2 (1917), pp. 129–168.
- [31] LGM de Souza, G Janiga, V John, and D. Thévenin. “Reconstruction of a distribution from a finite number of moments with an adaptive spline-based algorithm”. In: *Chemical Engineering Science* 65 (2010), pp. 2741–2750.

Zusammenfassung

In dieser Arbeit geht es um die numerische Simulation einer Rohrströmung, wobei das Medium eine Dispersion/Suspension bestehend aus Ethanol (fluide Phase) und Urea-Partikeln ist. Dabei werden die Phänomene Partikelwachstum, Nukleation und Aggregation berücksichtigt, wobei die Aggregation den größten Einfluss hat. In einem Experiment wurden detaillierte Untersuchungen dazu unternommen und dienen als Basis zur Validierung der numerischen Ergebnisse.

Mathematisch wird diese Rohrströmung durch sieben Gleichungen beschrieben, die zusammen ein Populationsbilanzsystem bilden, nämlich den Navier-Stokes-Gleichungen (drei Gleichungen für die Geschwindigkeiten und die Kontinuitätsgleichung), je einer nicht-linearen Konvektions-Diffusions-Reaktionsgleichung für die Temperatur und die Konzentration und einer Populationsbilanzgleichung für die Partikelverteilungsdichte. Dabei entspricht die Partikelverteilungsdichte einer Zähldichte, die, abgesehen von Ort und Zeit, auch von einer zusätzlichen inneren Variablen abhängt.

Zu Beginn der Arbeit werden die einzelnen Gleichungen zunächst hergeleitet und anschließend durch eine problemangepasste Wahl der Koordinaten vereinfacht. Dadurch verringert sich die Raumdimension aller Gleichungen um eins und man erhält eine analytische Lösung für das Strömungsfeld. Schließlich bleiben zwei nicht-lineare, konvektionsdominante partielle Differentialgleichungen für die Temperatur und Konzentration übrig. Die Partikelverteilungsdichte wird durch eine partielle Integro-Differentialgleichung beschrieben, da die Aggregation durch ein Funktional modelliert wird.

Das Hauptziel der Arbeit ist die numerische Lösung der Populationsbilanzgleichung, wofür eine finite Volumenmethode (FVM) implementiert wurde. Dies erfolgte in dem Forschungsprogramm MooNMD, welches an dem Weierstraß Institut für Angewandte Analysis und Stochastik entwickelt wird. Zur Lösung der anderen beiden Gleichungen wurden zugeschnittene Verfahren verwendet die bereits implementiert waren. Ein effizientes Verfahren zur Auswertung des Aggregationsintegrals war ebenfalls vorhanden.

Die finite Volumenmethode wird nach deren Beschreibung an konvektionsdominanten Konvektions-Diffusions-Reaktionsgleichungen verifiziert. Dabei wurde ein exponentiell angepasstes Aufwindverfahren implementiert, welches exemplarisch eine bessere Konvergenzordnung erzielt als ein einfaches Aufwindverfahren. Schließlich wird die numerische Lösung des Populationsbilanzsystems diskutiert. Da eine analytische Lösung nicht existiert, werden experimentelle Ergebnisse zur Validierung verwendet. Es stellt sich heraus, dass die numerisch erzielte Approximation die experimentellen Ergebnisse nicht genau genug wiedergibt, wobei die Ursache nicht festgestellt werden konnte. Dennoch kann es als Basis für weitere Untersuchungen dienen, da die Konvektions-Diffusionsgleichungen erfolgreich damit simuliert wurden. So kann z. B. eine Erweiterung zu drei Raumdimensionen vorgenommen werden sowie eine Anpassung an komplexe Geometrien.